A global timing mechanism regulates cell-type specific wiring programs

Saumya Jain[1,2,4], Ying Lin[1,3,4], Yerbol Z. Kurmangaliyev[2], Javier Valdes-Aleman[1,2], Samuel A. LoCascio[1], Parmis Mirshahidi[1], Brianna Parrington[1], and S. Lawrence Zipursky[1,2,*]

[1]Department of Biological Chemistry, University of California, Los Angeles, USA. [2]Howard Hughes Medical Institute, David Geffen School of Medicine, University of California, Los Angeles, USA. [3]Molecular Biology Institute, University of California, Los Angeles, USA. [4]These authors contributed equally to this work. [*]e-mail: lzipursky@mednet.ucla.edu

The assembly of neural circuits is dependent upon precise spatiotemporal expression of cell recognition molecules[1–6]. Factors controlling cell-type specificity have been identified[7–9], but how timing is determined remains unknown. Here we describe the induction of a cascade of transcription factors by a steroid hormone (Ecdysone) in all fly visual system neurons spanning target recognition and synaptogenesis. We demonstrate through single cell sequencing that the Ecdysone pathway regulates the expression of a common set of targets required for synaptic maturation and cell-type specific targets enriched for cell surface proteins regulating wiring specificity. Transcription factors in the cascade regulate the expression of the same wiring genes in complex ways, including activation in one cell-type and repression in another. We show that disruption of the Ecdysone-pathway generates specific defects in dendritic and axonal processes and synaptic connectivity, with the order of transcription factor expression correlating with sequential steps in wiring. We also identify shared targets of a cell-type specific transcription factor and the Ecdysone pathway which regulate specificity. We propose neurons integrate a global temporal transcriptional module with cell-type specific transcription factors to generate different cell-type specific patterns of cell recognition molecules regulating wiring.

MAIN

17 Animal behavior is dependent upon the formation of neural circuits with high fidelity.
18 Many cell-surface proteins, particularly of the Immunoglobulin (Ig), Leucine-Rich Repeat and
19 Cadherin families, promote interactions between neurons during circuit assembly[1,2]. How does a
20 limited set of cell-surface protein coding genes (~10^3 genes in fruit fly[10]) specify a much larger
21 number of synapses (~10^7 synapses amongst ~10^5 neurons in fly brain[11])? This is made possible
22 by the use of several developmental strategies including the reuse of the same molecules to
23 determine multiple, spatially and temporally separated neuron-neuron interactions[3,4,6,12]. Wiring
24 specificity, thus, relies on genetic programs which regulate the cell-type and temporal specificity
25 of genes encoding recognition molecules. Many programs that define cell-type specificity have
26 been described[7–9]. Here we set out to discover how temporal specificity is determined.

27 Dynamic expression of wiring genes

28 We defined metrics for cell-type specificity and temporal dynamics for each gene using
29 our previously reported transcriptomic dataset of 97 neuron-types in the fly visual system across
30 seven developmental time points (24 – 96 hours after pupal formation (hAPF))[12] (Fig. 1a). This
31 period encompasses dendritic and axon terminal morphogenesis within target regions, selection of
32 appropriate synaptic partners and synaptogenesis. We assigned two scores to each gene: 1) Cell-
33 type variability score, which provides a measure of cell-type specificity; and 2) Temporal
34 dynamicity score, which provides a measure of changes in expression across developmental time
35 (see Methods, Fig. 1a, Extended data Table 2).

36 "Housekeeping" genes, such as ribosomal protein coding genes (e.g. RpL36), generally
37 have low scores on both scales, suggesting low variation in expression across cell-types and time.

38 Many transcription factors (TFs) display high cell-type variability but low dynamicity scores (e.g.
39 erm), consistent with their role in establishing and maintaining neuron types[6,12,13]. A previously
40 identified set of genes representing a pan-neuronal program demonstrate low variability scores and
41 a range of dynamicity scores (e.g. RNA-binding protein, Rbp9)[12]. Finally, we compiled a list of
42 cell surface molecules (CSMs) with previously described roles in wiring (and paralogs thereof),
43 into a group we hereafter refer to as 'wiring genes' (see Methods, Extended data Table 3), and
44 found that they have high cell-type variability and temporal dynamicity scores (e.g. beat-IIIc).
45 Dynamic, cell-type specific expression is consistent with previous reports for expression patterns
46 for these genes[5,6,12]. While cell-type specific TFs have been identified which control wiring genes,
47 what controls their temporal specificity remains unknown.

48 **A cascade of nuclear receptors is expressed in visual system neurons**

49 To identify candidates for temporal regulators, we focused on TFs with high dynamicity
50 scores (Fig. 1a, Extended data Table 2). These were enriched for nuclear receptors (GO term:
51 "nuclear receptor activity", p-value 9.3 X 10^{-5}; Reactome pathway analysis: "Nuclear Receptor
52 transcription pathway" p-value 8.3 X 10^{-10}; also see Extended data Table 4). Nuclear receptor TFs
53 (such as Hr3, Hr4 and ftz-f1) which exhibit high temporal dynamicity (Fig. 1a), are components
54 of a cascade of TFs activated by the steroid hormone Ecdysone (Fig. 1b). Indeed, the Ecdysone
55 Receptor (EcR) itself, as well as other TFs in this cascade are expressed in a synchronous way in
56 all neurons in the developing visual system (at the mRNA and protein level, Fig. 1b, c, Extended
57 data Fig. 1). This includes a synchronous change in isoform from EcR-B1 to EcR-A[14]. The timing
58 and order of expression of these TFs correlates with a mid-pupal pulse of Ecdysone[15–19] (Fig. 1b).
59 Consistent with control of dynamic gene expression, ATAC-Seq[20] at 40hAPF, 60hAPF and

60 72hAPF in L1 neurons (see Methods) identified an enrichment for predicted binding sites for EcR,
61 Hr3 and Ftz-f1 in regions with dynamic patterns of chromatin accessibility[21] (Extended data Fig.
62 2, Extended data Table 5). Although these TFs are expressed in all neurons (Fig. 1b , c), they are
63 known in other contexts to regulate a cell-type specific set of genes[22]. These observations raised
64 the possibility that the Ecdysone-pathway has been co-opted as a temporal regulator to control the
65 dynamic and cell-type specific expression of wiring genes.

66 **EcR controls neurite terminal morphology and synapse distribution**

67 To test the role of the Ecdysone-pathway in wiring, we sought tools available for disrupting
68 the pathway. Given the proximity of the EcR gene to the centromere and the lethality of whole
69 animal mutants, phenotypic analysis using null-mutants is difficult to perform across cell-types
70 (see mosaic analysis with *EcR* mutants in L5 below). We thus, began by expressing a widely used
71 dominant-negative allele of EcR, EcR^{DN} (mutant with ligand-binding defect[23], EcR-B1^{W650A}), in a
72 range of neuron-types arborizing in different neuropils and layers using the GAL4-UAS system
73 (Fig. 2a, Extended data Fig. 3). Targeted expression of EcR^{DN} led to profound defects in axonal
74 and/ or dendritic branching across all neuron-types tested, namely lamina neurons (L1-L5), T4/T5,
75 Mi4 and Dm4 (Fig. 2, Extended data Fig. 3). EcR^{DN}-induced defects in L1-L5 arborization were
76 also seen with EcR-RNAi and could be largely rescued by overexpression of EcR-B1 from a cDNA
77 transgene (Extended data Fig. 3a).

78 We also observed that expression of EcR^{DN} in lamina neurons led to a redistribution of
79 their presynaptic sites in the lamina neuropil from strictly proximal to more distal regions of the
80 lamina (Fig. 2e). *DIP-β* mutants have been shown to produce a similar phenotype[24], and via
81 scRNA-Seq experiments described below, we identified DIP-β as a target of EcR in L4 neurons

82 (Extended data Fig. 4a, b). That DIP-β is directly regulated by EcR, is consistent with the presence
83 of a strong EcR binding site within the first intron of DIP-β (see Methods, Extended data Fig. 4c).
84 Thus, EcR controls dendritic and axonal terminal morphology and presynaptic site distribution
85 across cell-types in the lamina, medulla and lobula plate.

86 **Different EcR pathway TFs regulate specific steps in L5 wiring**

87 We next sought to investigate roles for the EcR-pathway at different steps in wiring of a
88 single neuron-type. L5 axon terminals target to medulla layer M5 during early pupal
89 development[25,26], then arborize in M1 (between 48hAPF and 60hAPF), followed by extension of
90 these arbors from M1 to M2 (between 75hAPF and 90hAPF) (Fig. 2f).

91 Targeted expression of EcR^{DN} in developing L5 neurons did not disrupt targeting to the
92 M5 layer, which is completed prior to the mid-pupal Ecdysone pulse. However, it led to a complete
93 lack of branches in M1/M2 (Fig. 2g, Extended data Fig. 5a). To verify the role of EcR in
94 establishing M1/M2 arbors, we generated a conditional null-allele for EcR using the FlpStop
95 technology[27] ($EcR^{FlpStop}$, see Methods, Extended data Fig. 5b). Similar to EcR^{DN}, we saw loss of
96 M1/M2 arbors in: 1) $EcR^{FlpStop}$ over a frameshift mutation in the ligand binding domain
97 ($EcR^{FlpStop/M554fs}$); 2) Heterozygous L5 neurons ($EcR^{FlpStop/+}$ or $EcR^{M554fs/+}$); and 3) knock-down of
98 EcR via RNAi. EcR mutants were phenocopied by a homozygous hypomorphic allele of *usp*
99 (usp^{R160H}). This gene encodes a cofactor which functions with EcR in different developmental
100 contexts[28,29] (Fig. 2g). By contrast to its role in promoting branching in M1/M2 medulla layers,
101 EcR suppresses L5 branching in the lamina (Fig. 2h). Wildtype L5 neurons (unlike L1-L4 neurons)
102 do not elaborate branches in the lamina[30]. However, in response to either EcR RNAi or EcR^{DN},

103 robust ectopic branching (similar in appearance to normal L1-L3 dendrites) was observed in the
104 lamina.

105 While disruption of EcR activity blocks step 1 and step 2, knock-down of TFs downstream
106 of EcR, Hr3 or Ftz-f1, selectively disrupts step 2 (Fig. 2g, Extended data Fig. 5a). These findings
107 are consistent with EcR regulating the expression of genes that promote extension of arbors into
108 M1 and that Hr3 and Ftz-f1 execute a distinct developmental step ~ 24 hours later (Fig. 2g),
109 promoting extension of arbors from M1 into M2. As Hr3 directly regulates *ftz-f1*[16] (Fig. 1b, see
110 Extended data Fig. 10), Ftz-f1 may act alone or in combination with Hr3, to regulate the expression
111 of genes required for branching in M2. Loss of Hr4, another TF directly downstream of EcR,
112 results in ectopic branches terminating in M5 (Fig. 2g, Extended data Fig. 5a). By contrast to the
113 medulla, suppression of branching in the lamina relies on Hr3, but not Ftz-f1 (Fig. 2h, i).

114 To see if the Ecdysone-pathway also affects communication between L5 and its
115 postsynaptic partners, we used an L5-specific Gal4 to express Chrimson with or without EcR^{DN}
116 and recorded Ca^{2+} responses in different postsynaptic cells (using GCaMP6s) upon activation of
117 Chrimson by light. Given the near complete loss of M1 arbors with EcR^{DN}, we focused on L5
118 postsynaptic partners in the M5 layer, Dm13 and Tm3[31]. Optogenetic stimulation of
119 EcR^{DN}-expressing L5 neurons led to a stronger response in Dm13 (Fig. 2j), while responses from
120 Tm3 remained unchanged (Extended data Fig. 6a). A postsynaptic neuron-type specific change in
121 GCaMP6s response is consistent with perturbation of L5 synaptic connectivity upon disruption of
122 the Ecdysone-pathway.

123 In summary, the Ecdysone-pathway sculpts L5 connectivity in multiple ways during
124 development, including affecting branches at different times, in different ways and within distinct
125 subcellular domains (see summary in Figure 2i).

126 **The EcR cascade regulates pan-neuronal and cell-type specific genes**

127 To identify genes regulated by the EcR cascade, we focused on lamina neurons (L1-L5).
128 These were enriched by Fluorescence-activated cell sorting[32] using a pan-lamina marker and
129 profiled using a single-cell RNA-Seq (scRNA-Seq) based approach similar to the one used in
130 Kurmangaliyev *et al*[12]. Transcriptional profiles of wildtype lamina neurons determined this way
131 were similar to the ones determined from dissociated whole optic lobes[12] (Extended data Fig. 7).
132 We then profiled the transcriptomes of EcR^{DN}, EcR RNAi or Hr3 RNAi-expressing lamina neurons
133 and controls by scRNA-Seq at four timepoints (24hAPF, 48hAPF, 72hAPF and Adult, see
134 Extended data Fig. 7a)[12].

135 By comparing the transcriptomes of wildtype and EcR^{DN}-expressing lamina neurons, we
136 identified 872 downregulated and 517 upregulated genes in EcR^{DN}-expressing cells (fold change
137 > 2, p-value < 0.05) (Fig. 3a; Extended data Fig. 8). Genes affected by EcR^{DN} are similar to the set
138 of genes affected by EcR RNAi, though the latter is significantly less effective at blocking the
139 Ecdysone pathway in this context (Extended data Fig. 9, 11a, c, e). Hr3 RNAi also has a similar
140 effect on gene expression as EcR^{DN}, especially at later time points (Extended data Fig. 10, 11b, d,
141 e) consistent with the genetic relationship between EcR and Hr3 (Fig. 1b). In contrast to L1 and
142 L3-L5, EcR^{DN} had modest effects on gene expression in L2, consistent with lower EcR^{DN}
143 expression in L2 neurons at 48hAPF using the pan-lamina GAL4 driver (Extended data Fig. 8b –
144 d, f). Thus, the EcR pathway regulates hundreds of genes in developing lamina neurons.

145 Analyses of the targets of the Ecdysone-pathway revealed that this pathway: 1) can both
146 activate and repress gene expression (Fig. 3a, c, d, Extended data Fig.12); 2) does not affect cell-

147 fate (Extended data Fig. 8e, 9e, 10e); and, 3) controls a larger number of genes with cell-type
148 specific, dynamic expression than expected by chance (one-sided Fisher's exact test, p-value =
149 0.005, Fig. 3b). Together, these observations establish that the Ecdysone-pathway controls
150 different sets of genes expressed in specific cell-types in a dynamic fashion. Importantly, we found
151 many dynamic genes to not be affected by EcR mutants, suggesting roles for other temporal
152 regulators as well (see Discussion, Fig. 3a, Extended data Fig. 11c, d, 12d).

153 Gene ontology analysis revealed that targets of the EcR pathway were enriched for genes
154 required for mitochondrial ATP biogenesis and neurotransmitter loading into synaptic vesicles
155 (see 'proton transport', Fig. 3b, c, Extended data Fig. 13b, Extended data Table 2), processes
156 required for synapse development, function or both[33–36]. Importantly, they have low cell-type
157 variability scores, and are thus likely regulated by the Ecdysone-pathway across neuron-types (Fig.
158 3b, also see common targets, Fig. 3a).

159 **Control of cell-type specific wiring genes**

160 The targets of EcR are also enriched for genes encoding CSMs, including wiring genes
161 (Fig. 3b, c). As opposed to genes required for ATP-synthesis and vacuolar ATPases, CSMs and
162 wiring genes regulated by the Ecdysone-pathway are largely composed of targets with cell-type
163 specific expression (Specific targets, Fig. 3a, b). These genes can be repressed in one cell-type and
164 activated in another (see dpr17 in L1 and L3, Fig. 3d), and can be regulated at different times in
165 different cell types (e.g. dpr10 in L1 and L5). In some cases, bidirectional changes in gene
166 expression resulted from activation by EcR, followed by repression by Hr3, indicative of a form
167 of feedback inhibition (e.g. see dpr10 and dpr15 in L1 and dpr17 in L3, Fig. 3d). Thus, activation
168 and repression by different Ecdysone-pathway TFs control cell-type and temporally specific
169 patterns of gene expression of wiring genes.

170 To assess if genes encoding CSMs affected by disruption of EcR activity are responsive to
171 hormone, we looked at the expression of some of these genes by controlling availability of
172 Ecdysone in *ex vivo* preparations. We modified a protocol developed by Özel *et al*, wherein brains
173 are removed from pupae (at 22hAPF) prior to the mid-pupal Ecdysone pulse, and then incubated
174 in media with or without the active form of Ecdysone, 20 Hydroxyecdysone[37] (20E, Extended data
175 Fig. 14a, see Methods). Consistent with scRNA-Seq data, the expression of several targets of EcR
176 depends upon inclusion of ligand in the media (Fig. 3e, Extended data Fig. 14b).
177 Together, these findings indicate that the Ecdysone-pathway, expressed in a common
178 temporal fashion in all neurons, regulates genes required for proper circuit formation in different
179 cell types in temporally specific ways.

180 **Erm and EcR co-regulate wiring genes in L3**

181 We next sought evidence that cell-type specific wiring programs are co-regulated by cell-
182 type specific and EcR pathway TFs. Here, we focused on a conserved TF, Erm (Fezf1/2 in
183 mammals) which is expressed in post-mitotic L3 neurons throughout development, but not other
184 lamina neurons, and controls several L3-specific wiring programs[32,38]. Though Erm is expressed
185 in a largely stable fashion throughout development, many of its known targets[38,39] (including
186 wiring genes) show dynamic expression (Fig. 4a). Interestingly, genes co-regulated by Erm and
187 EcR are enriched for dynamic genes (one-sided Fisher's exact t-test, p-value = 0.0331, see
188 Methods). Additionally, EcR pathway TFs are expressed sequentially in developing L3 neurons.
189 Together, these observations are consistent with Erm and the Ecdysone-pathway acting together
190 to determine the spatiotemporal expression patterns of wiring genes in L3.

191 L3 neurons non-cell autonomously control the targeting of R8 neurons to the M3 layer.
192 Netrin, which requires both Erm[38] and EcR for proper dynamic expression in L3 (Fig. 3e, Extended
193 data Fig. 16), is required for adhesion to the M3 layer, but not for recognition of the layer as its
194 target. Indeed, in *netrin* mutants R8s target to the appropriate later but then retract to distal layers
195 of the medulla[40]. While some R8s retract to distal medulla in *erm* and *EcR* mutants, most terminate
196 beyond M3[38] (Fig. 4b, d, Extended data Fig. 15b). This is consistent with Erm and EcR acting
197 together to control M3 target layer recognition and subsequent netrin-dependent stabilization. R8
198 terminals extending into deeper layers also contain ectopic presynaptic sites and show a modest
199 overall decrease in synapse number (Fig. 4c, Extended data Fig. 15a), consistent with defects in
200 R8 synaptic connectivity. We thus speculated that in addition to netrin, other genes co-regulated
201 by EcR and Erm (see Extended data Fig. 16) control R8 targeting.
202 To identify regulators of R8 targeting, we performed an RNAi screen for 12 genes co-
203 regulated by EcR and Erm (Fig. 4a, d, Extended data Fig. 15b, c, Extended data table 7, 8). Of
204 these, RNAi for beat-IIa, CG4822, CG6044 and Tpr2, led to R8 targeting past the M3 layer (Fig.
205 4d). Beat-IIa and CG6044 are members of the Ig superfamily, a class of genes known to mediate
206 cell recognition[1,2]. Tpr2 regulates the activity of steroid hormone receptors in mammals, and may
207 play an analogous role in regulating EcR-pathway TFs. Indeed, as in mammals where either
208 overexpression or knock-down of Tpr2 results in reduced hormone receptor activity[41,42], Tpr2
209 overexpression in L3 neurons phenocopies Tpr2 RNAi (Fig. 4d). And finally, CG4822, which
210 belongs to a subfamily of ABC transporters involved in cholesterol and steroid efflux, is also
211 implicated in steroid regulation[43,44].
212 Together these data indicate that the EcR-pathway and Erm co-regulate the spatiotemporal
213 specificity of several genes in L3 required for proper R8 wiring, including genes regulating steroid

214 abundance or steroid receptor function (CG4822 and Tpr2), genes encoding Ig superfamily
215 proteins (Beat IIa and CG6044) and secreted proteins (NetA and B) required for targeting to and
216 stabilization of R8 growth cones in M3.

217 **Discussion**

218 Wiring an animal brain requires precise cell-type and temporally specific expression of cell
219 recognition proteins[3–5,32,45]. The Ecdysone-pathway functions as a temporal regulator of major
220 developmental transitions, including larval molts and metamorphosis, as well as controlling
221 sequential divisions of postembryonic neuroblasts and neuronal re-modelling[15,22,46–48]. Here we
222 demonstrate that the EcR cascade has been co-opted for the temporal regulation of neuron-type
223 specific wiring programs within the developing neuropil. Neuron-type specificity in this case is,
224 at least in part, determined by the activity of cell-type specific TFs. The ability of the EcR cascade
225 to function as a flexible temporal regulatory module may be similar to modules regulating spatial
226 patterning (e.g. Hox genes and BMP/Wnt/Hh pathways[49–51]) which act in context-dependent ways
227 to generate different morphological outcomes in many different developmental contexts.

228 Global pathways, including other steroid and peptide hormones, waves of stimulus
229 independent neural activity, sensory experience as well as local intercellular interactions contribute
230 to wiring more broadly in controlling temporal aspects of development in the vertebrate and
231 invertebrate CNS (Fig. 4e)[52–57]. As in the EcR pathway in the fly visual system, these temporal
232 signals may also alter the activity of broadly expressed TFs (e.g. via phosphorylation) which
233 combine with cell-type specific TFs to control the expression of cell surface molecules regulating
234 synaptic connectivity.

Fig.1

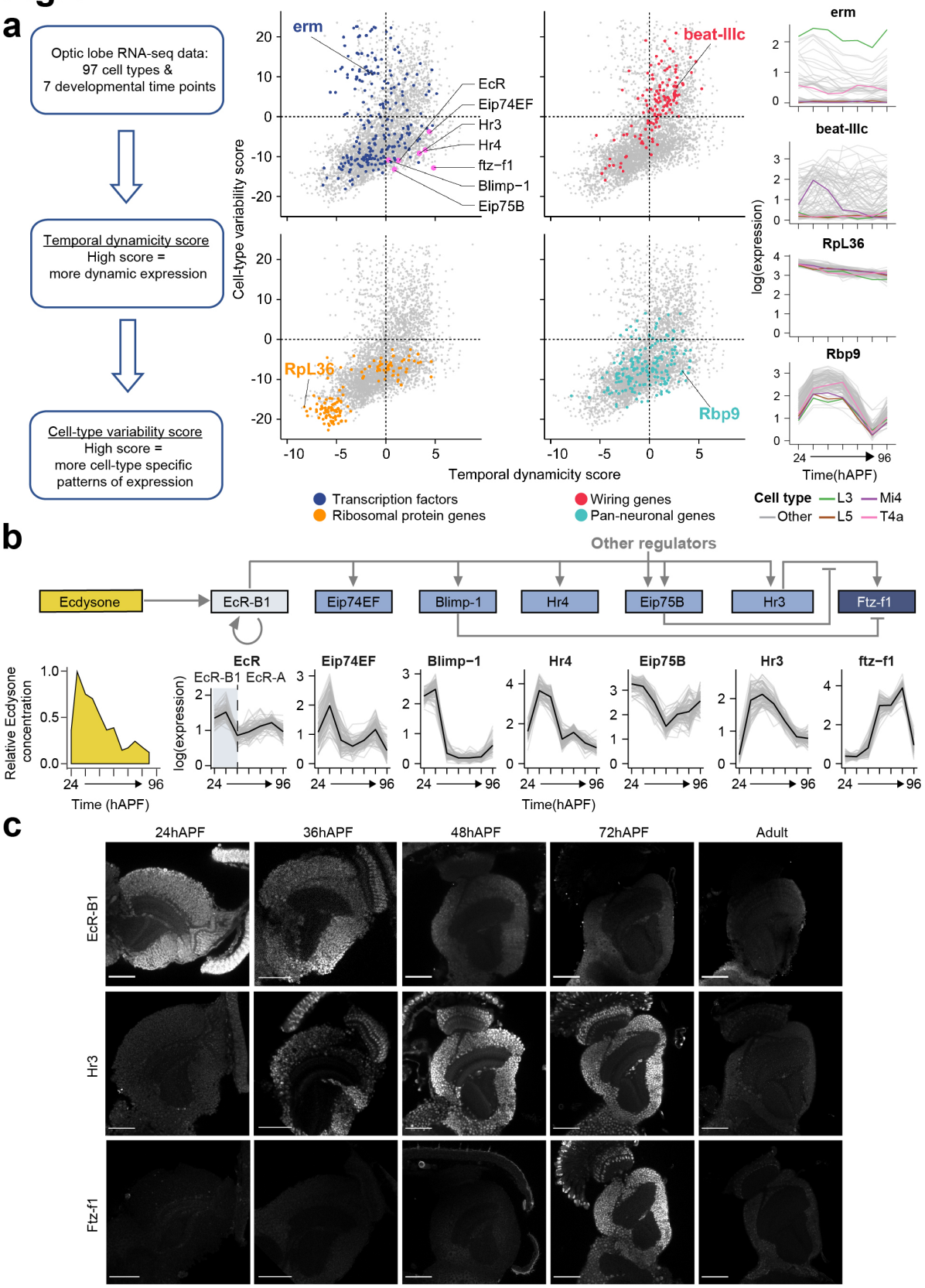
a
Optic lobe RNA-seq data:
97 cell types &
7 developmental time points
Temporal dynamicity score
High score =
more dynamic expression
Cell-type variability score
High score =
more cell-type specific
patterns of expression
erm
EcR
Eip74EF
Hr3
Hr4
ftz−f1
Blimp−1
Eip75B
beat-IIIc
RpL36
Rbp9
Cell-type variability score
Temporal dynamicity score
log(expression)
Time(hAPF)
Transcription factors
Ribosomal protein genes
Wiring genes
Pan-neuronal genes
Cell type
L3
Mi4
Other
L5
T4a
b
Other regulators
Ecdysone
EcR-B1
Eip74EF
Blimp-1
Hr4
Eip75B
Hr3
Ftz-f1
Relative Ecdysone concentration
Time (hAPF)
EcR-B1
EcR-A
log(expression)
Time(hAPF)
c
24hAPF
36hAPF
48hAPF
72hAPF
Adult
EcR-B1
Hr3
Ftz-f1

235 **Fig. 1. | Dynamic expression of wiring genes and Ecdysone pathway TFs. a,** Plots showing
236 Cell-type variability and Temporal dynamicity scores calculated using data from Kurmangaliyev
237 *et al.,* 2020[12]. Each plot highlights genes belonging to the indicated gene group. Right, expression
238 of one gene from each group, highlighting expression in L3, L5, Mi4, T4a neuron-types.
239 Transcription factors of the Ecdysone-pathway are highlighted (pink) in top-left plot. **b,** Ecdysone-
240 pathway showing a subset of known genetic interactions. Relative concentration of Ecdysone over
241 development is shown (adapted from Pak and Gilbert, 1987[19]). Line plots: each grey line is
242 expression in one neuron-type. Black line is mean across all neuron-types. Isoform change from
243 EcR-B1 to EcR-A is highlighted (also see Extended data Fig. 1). All expression plots: time in
244 hours after pupa formation (hAPF). All expression is log expression values from Kurmangaliyev
245 *et al.* **c,** Images showing immunostaining for EcR-B1, Hr3 and Ftz-f1 at the indicated time points.
246 Scale bar, 50μm.

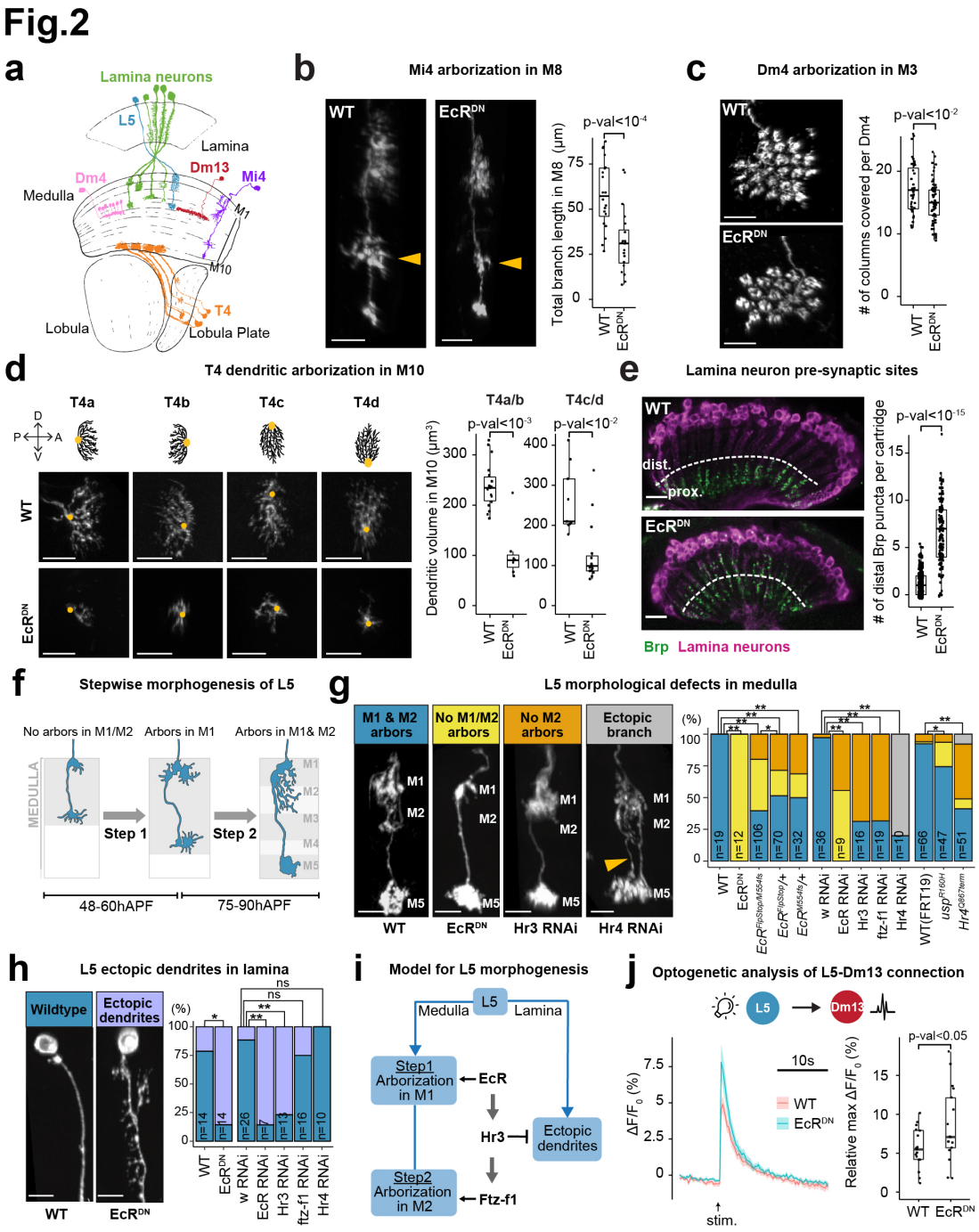

247 **Fig. 2. | Ecdysone-pathway TFs control multiple aspects of wiring. a,** Schematic of Lamina
248 (L1-L5), Mi4, Dm4, Dm13 and T4. **b,** Morphology of Mi4 ± EcR^{DN}. Yellow arrowhead: M8 layer.
249 Scale bar, 10µm. Total branch length in M8 is quantified. (WT, 20 neurons, 3 animals; EcR^{DN}, 20
250 neurons, 4 animals). **c,** Morphology of Dm4 ± EcR^{DN}. Total number of columns covered/ neuron

251 is quantified. (WT, 39 neurons, 5 animals; EcR^{DN}, 61 neurons, 5 animals). **d,** Schematic of
252 dendrites of T4 a-d subtypes. Dorsoventral (D, V) and anterior-posterior (A, P) axes are shown.
253 Below, dendrite morphology ± EcR^{DN}. Orange dot, dendritic stalk. Scale bar, 10μm. Dendritic
254 volume for T4a, b and T4c, d subtypes is quantified. (WT, 18 T4a/b, 9 T4c/d neurons, 4 animals;
255 EcR^{DN}, 7 T4a/b, 15 T4c/d neurons, 5 animals). **e,** Lamina neuron (magenta) presynaptic sites (Brp,
256 green) in the lamina neuropil ± EcR^{DN}. Scale bar, 50μm. Distal Brp puncta/ cartridge is quantified.
257 (WT, 409 cartridges, 7 animals; EcR^{DN}, 153 cartridges, 6 animals.) **f,** Schematic of stepwise
258 morphogenesis of L5 arbors. **g,** L5 arborization defects and their distributions under the given
259 genotypes (also see Extended data Fig. 5a). **h,** L5 ectopic dendrite phenotype with quantification
260 under given genotypes. **g, i,** n = number of neurons (all conditions, animals ≥ 4). **g, h,** Scale bar,
261 5μm. **i,** Schematic showing roles for EcR, Hr3 and Ftz-f1 in L5 branching. **j,** GCaMP6s response
262 in Dm13 upon optogenetic stimulation of WT and EcR^{DN}-expressing L5 neurons. Amplitude of
263 peak response for each condition is given. (WT, 17 animals; EcR^{DN}, 17 animals.) **b - e, j,** p-values
264 (two-sided Student's t-test) are given. **g, h,** *, p-value (one-sided Fisher's exact test) < 0.05, ** p-
265 value < 0.001.

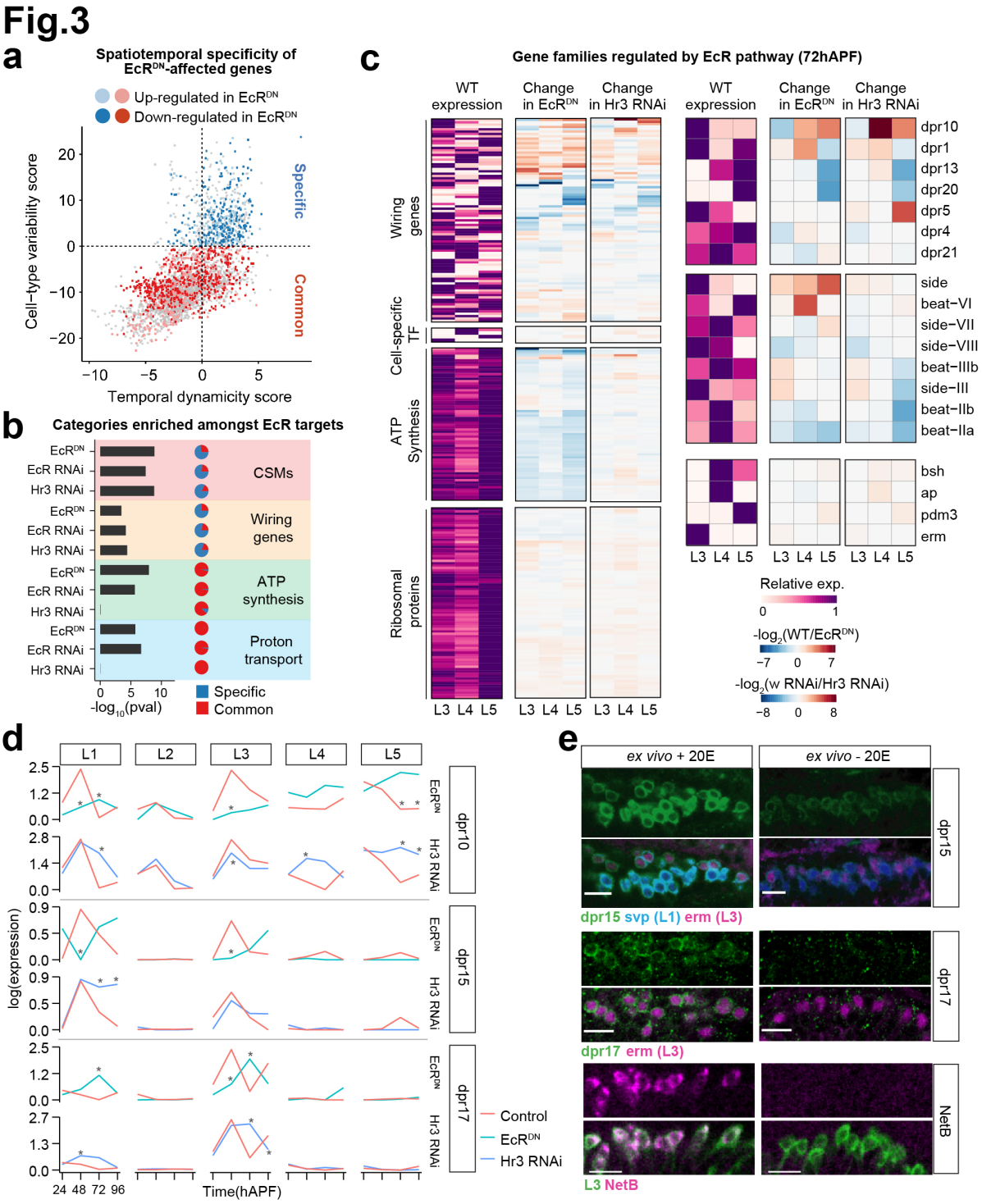

266 **Fig. 3. | Common and cell-type targets of the Ecdysone-pathway. a,** Cell-type variability vs

267 Temporal dynamicity plot for EcR^{DN}-affected genes (fold change > 2, p-value < 0.05). Cell-type

268 Specific (blue) and Common (red) targets are shown. Darker colors, genes reduced in EcR^{DN};

269 lighter colors, genes increased in EcR^{DN} (also see Extended data Fig. 11c, d). **b,** Gene groups
270 enriched amongst genes reduced in EcR^{DN}. Fraction of targets common to all neurons (red) and
271 neuron-specific (blue) targets in each category are shown as ratio of red to blue in small pie charts.
272 **c,** Relative WT expression at 72 hAPF (left), change in expression with EcR^{DN} (center), and change
273 in expression with Hr3 RNAi (right) shown as heat maps for all genes expressed in L3-L5 neurons
274 belonging to the specified gene categories at 72hAPF (also see Extended data Fig. 13a). Examples
275 of wiring genes (e.g. Dpr family, Side-Beat family) and cell-type specific transcription factors (e.g.
276 erm) are shown separately. **d,** dpr10, dpr15, dpr17 expression ± EcR^{DN} (above) and ± Hr3 RNAi
277 (below). * p-value < 0.05, fold change > 2. Expression is in log values. **e,** Staining for dpr15 and
278 dpr17 reporters (MiMIC lines, see Methods), and NetB (using anti-NetB antibody) in lamina
279 neuron cell-bodies ± 20 Hydroxyecdysone (20E – active form of Ecdysone) in the medium (also
280 see Extended data Fig. 14) in *ex vivo* preparations of pupal brains (see Methods). Note most NetB
281 protein accumulates in L3 growth cones in the M3 layer (not shown).

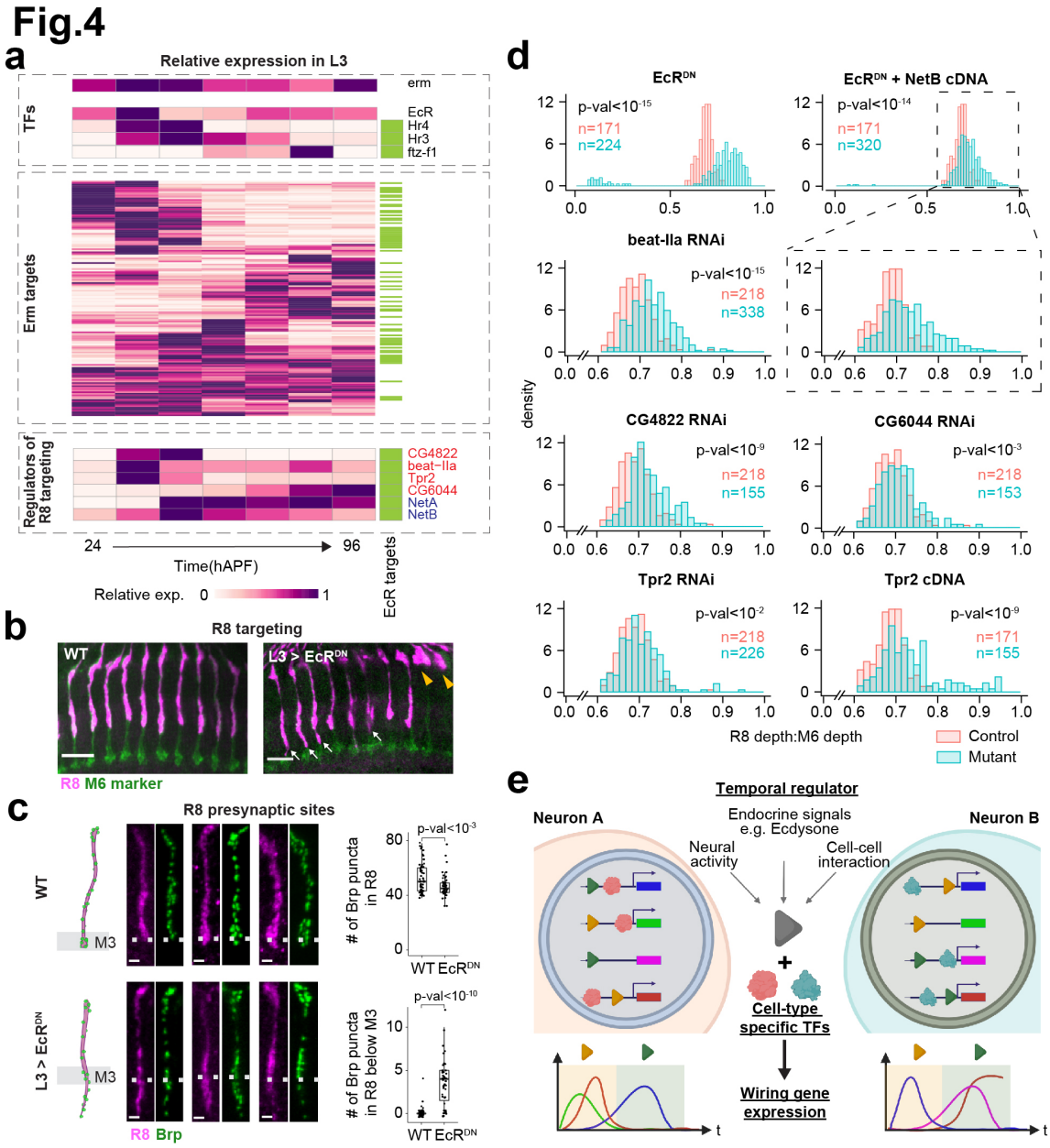

Fig. 4 | Screening EcR and Erm co-regulated genes for wiring regulators. a, Heatmap showing relative expression of erm, EcR-pathway TFs and Erm targets in L3 neurons[38,39]. Green box indicates genes affected by EcR^{DN} in L3 neurons. Genes that regulate R8 targeting are shown below as indicated. NetA and NetB (blue) are known regulators. Genes in red are identified in RNAi screen in this study. **b,** R8 axons ± EcR^{DN} expression in L3. Magenta, R8 neurons; green,

287 M6 marker (m24B10); yellow arrowheads, R8 axons terminating short of M3 and; white arrows,
288 R8 terminals extending beyond M3. Scale bar, 10μm. **c,** R8 presynaptic sites (Brp, green) ± EcR^{DN}
289 expression in L3. Right, quantification of Brp puncta number under the conditions shown. Scale
290 bar, 5μm. (WT, 58 neurons, 3 animals; EcR^{DN}, 47 neurons, 3 animals). **d,** Distributions of R8 axon
291 terminal depth (as in **b**) in control (red) or with expression of RNAi or cDNA (as shown, blue) in
292 L3 neurons. Numbers of neurons/ condition are given. All conditions, number of animals ≥ 3. p-
293 values (two-sided Student's t-test in **c,** Kolmogorov-Smirnov test in **d**) are given. **e,** Model for
294 cell-type specific temporal control of wiring gene expression (see text).

295 **REFERENCES**

296 1. Südhof, T. C. Towards an Understanding of Synapse Formation. *Neuron* **100**, 276--293 (2018).

297 2. Zipursky, S. L. & Sanes, J. R. Chemoaffinity Revisited: Dscams, Protocadherins, and Neural
298 Circuit Assembly. *Cell* **143**, 343--353 (2010).

299 3. Hassan, B. A. & Hiesinger, P. R. Beyond Molecular Codes: Simple Rules to Wire Complex
300 Brains. *Cell* **163**, 285--291 (2015).

301 4. Yogev, S. & Shen, K. Cellular and Molecular Mechanisms of Synaptic Specificity. *Annu Rev*
302 *Cell Dev Bi* **30**, 417--437 (2014).

303 5. Li, H. *et al.* Classifying Drosophila Olfactory Projection Neuron Subtypes by Single-Cell RNA
304 Sequencing. *Cell* **171**, 1206--1220.e22 (2017).

305 6. Özel, M. N. *et al.* Neuronal diversity and convergence in a visual system developmental atlas.
306 *Nature* 1–8 (2020) doi:10.1038/s41586-020-2879-3.

307 7. Hobert, O. Chapter Twenty-Five - Terminal Selectors of Neuronal Identity. in *Current Topics*
308 *in Developmental Biology* (ed. Wassarman, P. M.) vol. 116 455--475 (Academic Press, 2016).

309 8. Hong, W. & Luo, L. Genetic Control of Wiring Specificity in the Fly Olfactory System. *Genetics*
310 **196**, 17--29 (2014).

311 9. Dasen, J. S. & Jessell, T. M. Chapter Six Hox Networks and the Origins of Motor Neuron
312 Diversity. in *Current Topics in Developmental Biology* vol. 88 169--200 (Academic Press, 2009).

313 10. Larkin, A. *et al.* FlyBase: updates to the Drosophila melanogaster knowledge base. *Nucleic*
314 *Acids Res* **49**, D899–D907 (2020).

315 11. Scheffer, L. K. *et al.* A connectome and analysis of the adult Drosophila central brain. *Elife* **9**,
316 e57443 (2020).

317 12. Kurmangaliyev, Y. Z., Yoo, J., Valdes-Aleman, J., Sanfilippo, P. & Zipursky, S. L.
318 Transcriptional Programs of Circuit Assembly in the Drosophila Visual System. *Neuron* (2020)
319 doi:10.1016/j.neuron.2020.10.006.
320 13. Reilly, M. B., Cros, C., Varol, E., Yemini, E. & Hobert, O. Unique homeobox codes delineate
321 all the neuron classes of C. elegans. *Nature* **584**, 595–601 (2020).
322 14. Truman, J. W., Talbot, W. S., Fahrbach, S. E. & Hogness, D. S. Ecdysone receptor expression
323 in the CNS correlates with stage-specific responses to ecdysteroids during Drosophila and
324 Manduca development. *Dev Camb Engl* **120**, 219--234 (1994).
325 15. Riddiford, L. M., Cherbas, P. & Truman, J. W. Ecdysone receptors and their biological actions.
326 *Vitamins Hormones* **60**, 1--73 (2000).
327 16. White, K. P., Hurban, P., Watanabe, T. & Hogness, D. S. Coordination of Drosophila
328 metamorphosis by two ecdysone-induced nuclear receptors. *Sci New York N Y* **276**, 114--117
329 (1997).
330 17. Agawa, Y. *et al.* Drosophila Blimp-1 Is a Transient Transcriptional Repressor That Controls
331 Timing of the Ecdysone-Induced Developmental Pathway. *Mol Cell Biol* **27**, 8739--8747 (2007).
332 18. Rabinovich, D., Yaniv, S. P., Alyagor, I. & Schuldiner, O. Nitric Oxide as a Switching
333 Mechanism between Axon Degeneration and Regrowth during Developmental Remodeling. *Cell*
334 **164**, 170--182 (2016).
335 19. Pak, M. D. & Gilbert, L. I. A Developmental Analysis of Ecdysteroids During the
336 Metamorphosis of extitDrosophila Melanogaster. *J Liq Chromatogr* **10**, 2591--2611 (1987).
337 20. Buenrostro, J. D., Wu, B., Chang, H. Y. & Greenleaf, W. J. ATAC-seq: A Method for Assaying
338 Chromatin Accessibility Genome-Wide. *Curr Protoc Mol Biology Ed Frederick M Ausubel Et Al*
339 **109**, 21.29.1--9 (2015).

340 21. Imrichová, H., Hulselmans, G., Atak, Z. K., Potier, D. & Aerts, S. i-cisTarget 2015 update:
341 generalized cis-regulatory enrichment analysis in human, mouse and fly. *Nucleic Acids Res* **43**,
342 W57--W64 (2015).
343 22. Shlyueva, D. *et al.* Hormone-responsive enhancer-activity maps reveal predictive motifs,
344 indirect repression, and targeting of closed chromatin. *Mol Cell* **54**, 180--192 (2014).
345 23. Cherbas, L., Hu, X., Zhimulev, I., Belyaeva, E. & Cherbas, P. EcR isoforms in Drosophila:
346 testing tissue-specific requirements by targeted blockade and rescue. *Development* **130**, 271--284
347 (2003).
348 24. Xu, C. *et al.* Control of Synaptic Specificity by Establishing a Relative Preference for Synaptic
349 Partners. *Neuron* **103**, 865--877.e7 (2019).
350 25. Nern, A., Zhu, Y. & Zipursky, S. L. Local N-Cadherin Interactions Mediate Distinct Steps in
351 the Targeting of Lamina Neurons. *Neuron* **58**, 34--41 (2008).
352 26. Pecot, M. Y. *et al.* Sequential Axon-Derived Signals Couple Target Survival and Layer
353 Specificity in the Drosophila Visual System. *Neuron* **82**, 320--333 (2014).
354 27. Fisher, Y. E. *et al.* FlpStop, a tool for conditional gene control in Drosophila. *Elife* **6**, (2017).
355 28. Yao, T.-P., Segraves, W. A., Oro, A. E., McKeown, M. & Evans, R. M. Drosophila
356 ultraspiracle modulates ecdysone receptor function via heterodimer formation. *Cell* **71**, 63–72
357 (1992).
358 29. Yao, T. P. *et al.* Functional ecdysone receptor is the product of EcR and Ultraspiracle genes.
359 *Nature* **366**, 476--479 (1993).
360 30. Schwabe, T., Borycz, J. A., Meinertzhagen, I. A. & Clandinin, T. R. Differential Adhesion
361 Determines the Organization of Synaptic Fascicles in the Drosophila Visual System. *Curr Biol* **24**,
362 1304--1313 (2014).

363 31. Takemura, S. *et al.* Synaptic circuits and their variations within different columns in the visual
364 system of Drosophila. *Proc National Acad Sci* **112**, 13711--13716 (2015).
365 32. Tan, L. *et al.* Ig Superfamily Ligand and Receptor Pairs Expressed in Synaptic Partners in
366 Drosophila. *Cell* **163**, 1756--1769 (2015).
367 33. Lee, C. W. & Peng, H. B. The Function of Mitochondria in Presynaptic Development at the
368 Neuromuscular Junction. *Mol Biol Cell* **19**, 150–158 (2008).
369 34. Zhou, H. & Liu, G. Regulation of density of functional presynaptic terminals by local energy
370 supply. *Mol Brain* **8**, 42 (2015).
371 35. Rangaraju, V., Lauterbach, M. & Schuman, E. M. Spatially Stable Mitochondrial
372 Compartments Fuel Local Translation during Plasticity. *Cell* **176**, 73--84.e15 (2019).
373 36. Gowrisankaran, S. & Milosevic, I. Regulation of synaptic vesicle acidification at the neuronal
374 synapse. *Iubmb Life* **72**, 568–576 (2020).
375 37. Özel, M. N., Langen, M., Hassan, B. A. & Hiesinger, P. R. Filopodial dynamics and growth
376 cone stabilization in Drosophila visual circuit development. *Elife* **4**, e10721 (2015).
377 38. Peng, J. *et al.* Drosophila Fezf coordinates laminar-specific connectivity through cell-intrinsic
378 and cell-extrinsic mechanisms. *Elife* **7**, (2018).
379 39. Santiago, I. J. *et al.* Drosophila Fezf functions as a transcriptional repressor to direct layer-
380 specific synaptic connectivity in the fly visual system. *Proc National Acad Sci* **118**, e2025530118
381 (2021).
382 40. Akin, O. & Zipursky, S. L. Frazzled promotes growth cone attachment at the source of a Netrin
383 gradient in the Drosophila visual system. *Elife* **5**, e20762 (2016).
384 41. Moffatt, N. S. C., Bruinsma, E., Uhl, C., Obermann, W. M. J. & Toft, D. Role of the
385 Cochaperone Tpr2 in Hsp90 Chaperoning. *Biochemistry-us* **47**, 8203–8213 (2008).

386 42. Brychzy, A. *et al.* Cofactor Tpr2 combines two TPR domains and a J domain to regulate the
387 Hsp70/Hsp90 chaperone system. *Embo J* **22**, 3613–3623 (2003).
388 43. Klucken, J. *et al.* ABCG1 (ABC8), the human homolog of the Drosophila white gene, is a
389 regulator of macrophage cholesterol and phospholipid transport. *Proc National Acad Sci* **97**, 817–
390 822 (2000).
391 44. Suzuki, M., Suzuki, H., Sugimoto, Y. & Sugiyama, Y. ABCG2 Transports Sulfated Conjugates
392 of Steroids and Xenobiotics*. *J Biol Chem* **278**, 22644–22649 (2003).
393 45. Kurmangaliyev, Y. Z., Yoo, J., LoCascio, S. A. & Zipursky, S. L. Modular transcriptional
394 programs separately define axon and dendrite connectivity. *Elife* **8**, e50822 (2019).
395 46. Alyagor, I. *et al.* Combining Developmental and Perturbation-Seq Uncovers Transcriptional
396 Modules Orchestrating Neuronal Remodeling. *Dev Cell* **47**, 38--52.e6 (2018).
397 47. Uyehara, C. M. & McKay, D. J. Direct and widespread role for the nuclear receptor EcR in
398 mediating the response to ecdysone in Drosophila. *Proc National Acad Sci* **116**, 9893--9902
399 (2019).
400 48. Syed, M. H., Mark, B. & Doe, C. Q. Steroid hormone induction of temporal gene expression
401 in Drosophila brain neuroblasts generates neuronal and glial diversity. *Elife* **6**, e26287 (2017).
402 49. Altmann, C. R. & Brivanlou, A. H. Neural patterning in the vertebrate embryo. *Int Rev Cytol*
403 **203**, 447–482 (2001).
404 50. Briscoe, J. & Small, S. Morphogen rules: design principles of gradient-mediated embryo
405 patterning. *Development* **142**, 3996–4009 (2015).
406 51. Gaunt, S. J. Hox cluster genes and collinearities throughout the tree of animal life. *Int J Dev*
407 *Biol* **62**, 673–683 (2018).

408 52. Prezioso, G., Giannini, C. & Chiarelli, F. Effect of Thyroid Hormones on Neurons and
409 Neurodevelopment. *Horm Res Paediat* **90**, 73–81 (2018).
410 53. Miranda, A. & Sousa, N. Maternal hormonal milieu influence on fetal brain development.
411 *Brain Behav* **8**, e00920 (2018).
412 54. Akin, O. & Zipursky, S. L. Activity regulates brain development in the fly. *Curr Opin Genet*
413 *Dev* **65**, 8–13 (2020).
414 55. Ting, C.-Y. *et al.* Photoreceptor-Derived Activin Promotes Dendritic Termination and
415 Restricts the Receptive Fields of First-Order Interneurons in Drosophila. *Neuron* **81**, 830--846
416 (2014).
417 56. Mizumoto, K. & Shen, K. Two Wnts Instruct Topographic Synaptic Innervation in C. elegans.
418 *Cell Reports* **5**, 389–396 (2013).
419 57. Umemori, H., Linhoff, M. W., Ornitz, D. M. & Sanes, J. R. FGF22 and Its Close Relatives Are
420 Presynaptic Organizing Molecules in the Mammalian Brain. *Cell* **118**, 257–270 (2004).

421 **METHODS**

422 **Fly husbandry and stocks**

423 Maintenance and rearing of fly lines, as well as staging of pupae was done as described in
424 Tan *et al.*[32] Fly lines used in this work are listed in Supplementary Table 1.

425 **Data analyses of fly optic lobe RNA-seq**

426 *Measure of cell-type variability and temporal dynamicity for each gene*

427 RNA-seq data of developing fly optic lobe were generated by Kurmangaliyev *et al.*[12],
428 which contains 97 cell types covering 7 time points. For each gene, we assigned a cell-type
429 variability score by their cell-type specific expression and a temporal dynamicity score by their
430 expression changes over development. Cell-type variability score was calculated by the variance
431 of gene expression at each time point when the gene is expressed, and then the maximum variance
432 was normalized by the average expression across cell types that time point. Temporal dynamicity
433 score was calculated by the sum of the absolute changes between consecutive time points for each
434 cell type where the gene is expressed, and then the averaged value across cell types is normalized
435 by the average of their peak expression. Both scores were centered their mean to 0 and transformed
436 to natural log for visualization.

437 *Wiring genes*

438 Genes were designated to the category of 'wiring genes' if they satisfied the following
439 criteria: 1) they were amongst the top 50% of the highest expressed cell-surface or secreted
440 molecules in the developing optic lobe (from Kurmangaliyev *et al.*), 2) either themselves, or their
441 paralogs (DIOPT v8.0 score $\geq$ 4) had published roles in establishing neuronal morphology or
442 connectivity in *Drosophila*. Extended data Table 3 contains a list of wiring genes along with
443 references to published studies describing their roles in wiring.

444 *Gene Ontology and REACTOME analysis of dynamic TFs*

445 Dynamic TFs were defined as ones with temporal dynamicity score > 0 (see Fig. 1a,
446 Extended data Table 2). Gene ontology analysis was performed using GOrilla (http://cbl-
447 gorilla.cs.technion.ac.il) using dynamic TFs ranked on the basis of temporal dynamicity scores.
448 All enriched categories are given in Extended data Table 4. For REACTOME pathway analysis,
449 dynamic TFs were entered into the 'Analyze Data' tool on reactome.org
450 (https://reactome.org/PathwayBrowser/#TOOL=AT). Reactome pathway analysis for *Drosophila*
451 *melanogaster* was then run with default parameters.

452 **Bulk RNA-seq**

453 Bulk RNA-Seq analysis of L1 neurons at 40hAPF, 60hAPF and 72hAPF was performed
454 as in Tan *et al.*[32] At least 2 replicates were generated for each timepoint. A minimum of 2000 cells
455 were sorted for each experiment. cDNA libraries were created using the SMART-Seq2 protocol[58],
456 which were then sequenced together using the HiSeq4000 platform (paired-end 50bp). Raw fastq
457 reads files were mapped to FlyBase reference genome (release 6.29) using STaR (2.6.0) and only
458 uniquely mapped reads were collected. Genes with counts per million (CPM) ≥ 4 in more than 2
459 samples were used for normalization with R package edgeR (3.26.8). Gene expression was
460 quantified using RPKM units (Reads Per Kilobase of exon per Million reads mapped), calculated
461 based on reads in the sum of exons using customized scripts. The correlation between biological
462 replicates were calculated using Spearman correlation for top 500 genes with the highest variation
463 across all samples. Coverage tracks were generated by bamCoverage(3.5.1).

464 **Bulk ATAC-seq**

465 At least 8000 L1 neurons were FACS purified at 40hAPF, 60hAPF and 72hAPF as
466 described in Tan *et al*.[32] Biological duplicates were generated for each timepoint. ATAC-Seq
467 libraries were generated as per the following protocol, which was modified from the one described
468 in Buenrostro *et al*.[59]: 1) FACS purified cells were collected in 300ul 1X PBS and spun at 800xg
469 for 8' at 4°C. 2) Cell pellet was then directly resuspended in 50µl of a tagmentation enzyme mix
470 (25µl Nextera DNA library prep kit – Tagment DNA Buffer, 19µl Nuclease-free water, 5µl 1%
471 IGEPAL CA630, 1µl Nextera DNA library prep kit - Tagment DNA Enzyme) and incubated at
472 37°C for 30' with constant agitation at 400rpm. 3) DNA was purified from the tagmentation mixes
473 using the Qiagen minElute Reaction Cleanup Kit as per the manufacturer's protocol. 4) A 10µl
474 qPCR reaction was setup to determine the optimum number of amplification 455 cycles (similar
475 to Buenrostro *et al*.). 5) A larger PCR reaction (40µl) was then setup and PCR products in the 200-
476 500bp range were gel purified. 6) Steps 4 and 5 were repeated, this time with barcoded primers
477 (see Buenrostro *et al*.) to allow multiplexing of all libraries onto a single lane of HiSeq4000
478 (paired-end 50bp).

479 Raw fastq reads files were mapped to FlyBase reference genome (release 6.29) using
480 Bowtie2 (2.2.9) and uniquely mapped genes were kept. All samples were pooled together prior to
481 peak calling. Read start positions were shifted +4 or -5bp and used for peak calling using MACS2
482 (2.1.1) with parameters "-q 0.01 --nomodel --shift -100 --extsize 200". There were 26,122 peaks
483 identified. Then bedtools multicov (2.27.1) was used to sum the total reads within each peak
484 separately for each sample. Peaks with CPM ≥ 4 were used for counts normalization with edgeR.
485 Correlations between biological replicates were calculated using Spearman correlation for the top
486 500 peak regions with the highest variation of peak levels across all samples. Distribution of the
487 top 5000 peaks across different genomic features at 40hAPF, 60hAPF and 72hAPF was

488 determined using the R package ChIPseeker (1.20.0). Each ATAC peak was associated to the
489 nearest gene based on proximity to the transcription start site using ChIPseeker. To compare
490 change of ATAC-seq peak accessibility over time and change in expression of their nearest gene,
491 $\log_2$(fold change ATAC-seq peak read coverage) was plotted against $\log_2$(fold change expression
492 of nearest gene) for dynamic ATAC-Seq peak (Extended data Fig. 2b). Bulk RNA-Seq data was
493 used for this, as this transcriptome dataset had been generated for the same time points as for
494 ATAC-Seq. This was done separately for peaks differentially accessible between 40hAPF and
495 60hAPF (Extended data Fig. 2b (left)) and between 60hAPF and 72hAPF (Extended data Fig. 2b
496 (right)). Differential peak analysis was performed using edgeR. Fold-change> 2 and adjusted p-
497 value < 0.05 were chosen as the cutoffs to define peaks with differential accessibility between time
498 points (dynamic peaks).

499 Binding sites for the EcR-usp complex (motif: Jaspar MA0534.1), Hr3 (motif: Fly Factor
500 Survey, Hr46_SANGER_5) and Nr5a1, mammalian homolog of Ftz-f1 (motif: Jaspar 1540.1)
501 across the genome were identified using the PWMscan (https://ccg.epfl.ch/pwmscan/). Cutoff of
502 p-value < 10^{-5} were used to identify binding sites[60]. Enrichment of binding sites within different
503 sets of ATAC-Seq peaks (Extended data Fig. 2d) was done using Homer (v4.7) mergePeaks utility.
504 p-value ≤ 0.01 was considered as significantly more overlap than expected by chance.

505 **Calcium imaging**

506 Calcium imaging experiments were performed using a 3i VIVO Multiphoton upright
507 microscope (Intelligent Imaging Innovations) with a water immersion objective (W Plan-
508 Apochromat 20x/1.0 DIC, Zeiss). L5 neurons expressing CsChrimson (using 64B07 Gal4) were
509 photo-stimulated with a 1040 nm laser (SpOne-8, Spectra-Physics) coupled to a 2-photon Phasor

510 (Intelligent Imaging Innovations) to generate a holographic pattern to restrict the stimulation area.
511 GCaMP6s responses were recorded using an imaging laser tuned to 940 nm (Chameleon
512 Discovery, Coherent).

513 Experimental crosses were set in vials with fly food supplemented with all-trans retinal
514 (0.5 mM) and kept in the dark at 25 ºC. The brains of ≤ 5-day old adult flies were dissected in a
515 saline solution (135 mM NaCl, 5 mM KCl, 2 mM $CaCl_2.2H_2O$, 4 mM $MgCl_2.6H_2O$, 5 mM TES,
516 36 mM Sucrose, pH 7.15) and mounted dorsal side on a poly-L-lysine-coated coverslip. Typically,
517 the dissected brains were held for about 5 minutes before the start of the experiment to ensure a
518 stable basal calcium signal. The photo-stimulation hologram was restricted to a rectangular area
519 of 18 µm x 65 µm to roughly cover the middle third of the axon layer of L5 neurons in the medulla
520 layers 1-2. The experimental protocol consisted of three consecutive iterations of a 30 s resting
521 period and a 500 ms stimulation event. The stimulation laser power at the objective end was 335
522 mW, measured with a power meter (PM100D Thorlabs). GCaMP responses were recorded from a
523 single Z plane at 3.05 frames/s. This protocol was executed on both optic lobes when possible.

524 *Image processing*

525 The GCaMP image data were processed using custom macros in Fiji and analyzed using
526 custom code written in R. Briefly, a region of interest (ROI) was manually defined as the medulla
527 layers that include the sub-arbors of the neurons expressing GCaMP. The average pixel value
528 inside such ROI was measured across all time points for each sample. All fluorescence values were
529 reported relative to a fluorescence baseline (F_0) defined as the median pixel value of the
530 corresponding ROI during the entire imaging experiment. $\Delta F/F_0$ was calculated as $\Delta F/F_0 = (Ft –$
531 $F_0)/F_0$, where Ft is the mean fluorescence value of the ROI at a given time point. The relative
532 maximum ΔF/F0 was defined in a 10 s time window immediately after stimulation offset from

533 which the recent baseline (mean $\Delta F/F_0$ of the 6.5 s preceding stimulation onset) was subtracted.
534 Those failed individual trials in which there were no detectable responses were discarded. The
535 three individual stimulation events from left and right hemispheres trials were averaged to generate
536 a single response trace per animal.

537 **Multiplexed single cell transcriptomic analysis**

538 For transcriptomic analysis of developing wildtype lamina neurons, w; UAS-H2A-GFP;
539 9B08-Gal4/Tm6B, tb females were crossed with males from different DGRP backgrounds
540 (wildtype, see Supplementary Table 1 for list of DGRPs used). F1 prepupae were staged as in
541 Kurmangaliyev *et al.*[12] Males were only included in the analysis if no significant differences in
542 gene expression were found with female pupae of the same genotype and developmental time
543 point. Pupae corresponding to different developmental stages (see Extended data Fig. 7a) were all
544 dissected, dissociated and processed at the same time. Each developmental time point was
545 represented by ≥ 2 DGRP heterozygotes, and only one animal/ DGRP heterozygote was dissected.
546 Tissue dissociation, FACS and preparation of single-cell libraries using 10X Genomics Chromium
547 (v3) were carried out similar to Kurmangaliyev *et al.*, except that H2A-GFP expression was used
548 to enrich for lamina neurons. All libraries were sequenced on a NextSeq500 platform (single-end
549 75bp).

550 For transcriptomic analysis involving UAS EcR^{DN} (BDSC #6872), males carrying a single
551 DGRP autonomous chromosome – w; (UAS EcR^{DN} or UAS tdTom); DGRP/ Tm6b, tb were
552 crossed with w; UAS-H2A-GFP; 9B08-Gal4/Tm6B females. For experiments involving UAS EcR
553 RNAi (BDSC #9326) or UAS Hr3 RNAi (BDSC #27253), w; DGRP; (UAS wRNAi or UAS EcR
554 RNAi or UAS Hr3 RNAi)/ Tm6B, tb males were crossed with UAS Dcr2; UAS H2A-GFP; 9B08

555 Gal4/ Tm6B, tb females (see Extended data Fig. 7a and Supplementary Table 1). UAS tdTom
556 and UAS wRNAi were used as controls.

557 *scRNA-seq data pre-processing*

558 Raw fastq read files were processed using Cell Ranger (3.1.0) with default parameters.
559 Seurat V3 was used for all preliminary analyses. FlyBase reference genome (release 6.29) was
560 used for alignment and annotation. Profiled single cells were identified as coming from a particular
561 developmental time-point and genetic background based on the natural genomic variance within
562 the different parent DGRP lines. This was done using the pipeline described in Kurmangalyev *et*
563 *al.*[12], with the following modifications: the count of minor allele that equals to 2 among the
564 analyzed DGRP strains were used as genomic variants to assign the profiled single cells to different
565 DGRP parent lines. Only single cells with: 1) number of genes between 200 and 3000, 2) number
566 of mitochondrial transcripts < 20% of all transcripts, and 3) assignment to a unique DGRP parent
567 line; were used for all downstream analyses.

568 To identify different lamina neuron subtypes, all cells from a particular were integrated as
569 described in Seurat v3 workflow and then subjected to unsupervised clustering, thus disregarding
570 global temporal gene expression changes (similar to Kurmangaliyev *et al.*). Previously identified
571 lamina neuron subtype specific genes[32] were used to assign each cluster to a cell-type. All cell
572 cluster separations are visualized in tSNE plots. Cells not assigned to a lamina neuron-type cluster
573 were removed from subsequent analyses. Average expression for each gene for each cell-type at a
574 particular timepoint and genetic background was calculated using normalized expression values
575 prior to integration.

576 A global-scaling normalization used in Butler *et al.*[61] is used in all scRNA-seq analysis in
577 this paper. We normalize the gene expression measurement for each cell by the total expression
578 and multiply by scale factor 10000. All expression shown in figures are natural log transformed.

579 **Comparison of scRNA-Seq with published dataset**

580 For comparison of lamina neuron transcriptomes generated here with lamina neuron
581 transcriptomes generated in Kurmangaliyev *et al.*, 500 genes with the highest variance across all
582 cell types and all timepoints were used to calculate Spearman correlation.

583 **Differential gene expression analysis**

584 Wilcoxon rank-sum test (fold change > 2, adjusted p-value < 0.05) was used to identify
585 genes differentially expressed between timepoints, cell-types or as a consequence of EcR/ Hr3
586 perturbations. All fold change calculation used pseudo number 0.01.

587 **Enrichment analysis amongst EcR and Hr3 targets**

588 For each of the four categories shown in Fig. 4b, enrichment was calculated using Fisher's
589 exact test. Briefly, number of genes expressed in lamina neurons overlapping with genes in the
590 stated category vs other genes expressed in lamina neurons, was used to define a null hypothesis.
591 Then genes affected by EcR^{DN}, EcR RNAi or Hr3 RNAi were also divided into ones overlapping
592 with genes in the stated category, and ones that don't overlap. Number of genes in these two
593 categories, along with similar numbers from the null-hypothesis, were then used to create a 2X2
594 matrix, which was then subjected to Fisher's exact test.

595 Gene categories, Proton transport (proton transmembrane transport, GO:1902600) and
596 ATP synthesis (ATP metabolic process, GO:0046034) were initially identified from GO analysis
597 of targets of EcR^{DN} and EcR RNAi.

598 **Gene group analysis for EcR and Hr3 perturbation effect**

599 Prior to clustering, all average gene expression from scRNA-seq transcriptomic analysis
600 were normalized to maximum expression in each cell type across development. For each cell types,
601 the relative expression of each gene was used to perform k-means clustering to assign expressed
602 genes in different groups. The number of clusters for each cell type were determined by calculating
603 Within-Clsuter of Squared Errors (WSS) and finding where the difference of WSS in consecutive
604 cluster number first become less than 5. For Extended data Fig. 12, we presented the gene groups
605 with the most up-regulated or the most down-regulated or the unchanged gene expression after
606 expressing EcR^{DN} in each lamina neuron.

607 ***Ex vivo* culture of dissected brains**

608 We used a protocol similar to the one described in Özel *et al.*[37] Briefly, brains were
609 dissected from 22hAPF pupae in pre-warmed Schneider's medium (ThermoFisher #2172004) with
610 either 1:1000 dilution of 1mg/ml 20-HydroxyEcdysone (dissolved in 100% Ethanol, Sigma
611 H5142) or equivalent volume of 100% ethanol. Brains were then incubated in ~ 200ul of medium
612 ± 20-HydroxyEcdysone in 96 well plates for 26h at 25ºC in a humidified chamber. Thereafter,
613 brains were fixed, stained and imaged using the aforementioned protocols for
614 immunohistochemistry and microscopy (see Extended data Fig. 14a).

615 In the presence of 20-HydroxyEcdysone in the media, strong expression of EcR-B1 and
616 Hr3 is observed throughout the optic lobe, while no expression of Ftz-f1 is seen (Extended data
617 Fig. 14a). When 20-HydroxyEcdysone is omitted from the culture medium, no expression of Hr3
618 is seen (as expected), however weak induction of Ftz-f1 is observed. The transcriptional regulation
619 of ftz-f1 is not completely understood, and previous work has shown that ftz-f1 can be induced
620 even without Hr3 expression. Apart from Hr3, another target of EcR – Blimp-1 has also been
621 shown to regulate ftz-f1 expression by functioning as a repressor. Indeed, loss of Blimp-1 leads to
622 ftz-f1 expression[17]. In brains incubated without Ecdysone, the weak induction of ftz-f1 may be (in
623 part) due to lack of Blimp-1 expression.

624 **Immunohistochemistry and microscopy**

625 Immunohistochemistry and microscopy were performed as described in Xu *et al.*[62] with
626 the following modifications: 1) For experiments involving staining of presynaptic sites and L5
627 morphology, brains were fixed using glyoxal (3.12% glyoxal, 0.75% acetic acid and 20% ethanol,
628 pH adjusted to 5.0) for 30' at RT and then washed 3X with PBST. 2) All images were acquired
629 using an LSM880 confocal microscope.

630 Primary antibodies used in this study were: mAb24B10 (1:20, DSHB), rabbit anti-NetB
631 (1:500, gift from Akin Lab), rabbit anti-dsRed (1:400, Clontech 632496), chicken anti-GFP
632 (1:1000, Abcam ab13970), rat anti-Flag (1:200, Novus Biologicals, NBP1-06712), mouse anti-
633 EcR-B1 (1:20, DSHB AD4.4), mouse anti-EcR-A (1:10, DSHB 15G1a), rabbit anti-Hr3 (1:50, gift
634 from Thummel Lab), mouse anti-Svp (1:20, DSHB 5B11), rabbit anti-Erm (1:100, gift from Wang
635 Lab), rat anti-Bab2 (1:500, gift from Laski Lab), mouse anti-V5 (1:200, BioRad MCA1360),
636 guinea pig anti-Bsh (1:400, see Tan *et al.* 2015), guinea-pig anti-DIP-β (1:300, gift from Pecot

637 Lab). Secondary antibodies used in this study were: goat anti-mouse 488 (1:500, ThermoFisher A-
638 32723), goat anti-mouse 568 (1:500, ThermoFisher A-11031), goat anti-mouse 647 (1:500,
639 ThermoFisher A-21235), goat anti-chicken 488 (1:1000, ThermoFisher A-11039), goat anti-rabbit
640 568 (1:500, ThermoFisher A-11011), goat anti-guinea pig 647 (1:500, ThermoFisher A-21450),
641 goat anti-rabbit 647 (1:200, ThermoFisher A-32733), goat anti-rat 568 (1:500, ThermoFisher A-
642 11077), goat anti-guinea pig 568 (1:500, A-11075).

643 **Image analysis**

644 All images for figures were created using ImageJ (v2.1.0) or Imaris (v9.1.2). Details for
645 quantification of phenotypes are given below.

646 *R8 targeting*

647 Imaris (v9.1.2) was used to measure the distance of R8 terminals from the top of the
648 medulla (M0), as well as the distance of 6th medulla layer (M6) from the top of the medulla. The
649 latter was estimated using mAb24B10 staining, which labels R7 neurons that terminate in M6.
650 Values reported on the X-axis of Fig. 4d and Extended data Fig. 15b are (R8-M0)/ (M6-M0).

651 *L5 morphological defects*

652 Imaris was used to visualize individual neurons. Each neuron was then manually assigned
653 to one of the stated categories.

654 *Quantification of BRP puncta*

655 For lamina neuron presynaptic sites in the lamina: the distance between the proximal end
656 of the lamina and the distal end of the lamina was measured using Imaris individually for all lamina
657 cartridges. A line was drawn at the measured distance divided by 2. All BRP puncta more distal

658 of this line were counted manually. For R8 presynaptic sites: All Brp puncta were counted
659 manually.

660 **Other statistics**

661 One-sided Fisher's exact test was used to determine the enrichment of dynamic genes
662 (temporal dynamicity score > 0, calculated as in Fig. 1a, but specifically for L3) within common
663 targets of EcR and Erm as compared to targets of Erm alone. Targets of Erm were obtained from
664 Peng *et al*. and Santiago *et al.*[38,39].

665 For all box-plots, solid line depicts median, while the upper and lower bounds of the box
666 depict the third and first quantile of the data spread respectively.

667 Kolmogorov-Smirnov (KS) test (Fig. 4d, Extended data Fig. 15b, c), two-tailed Student's
668 t-test (Fig. 2b-e, 2j, 4c, Extended data Fig. 6, 8c, 15a), two-tailed Fisher's exact test (Fig. 2g, h,
669 Extended data Fig. 5a), one-tailed Fisher's exact test (Fig. 3b, Extended data Fig. 2d) were
670 performed using the following basic R functions (R 3.6.1) respectively: ks.test, t.test, fisher.test.
671 Raw data for all analyses is available upon request.

672 **Data and code availability**

673 All raw sequencing data and codes will be provided upon request. They will be made
674 publicly available prior to publication.

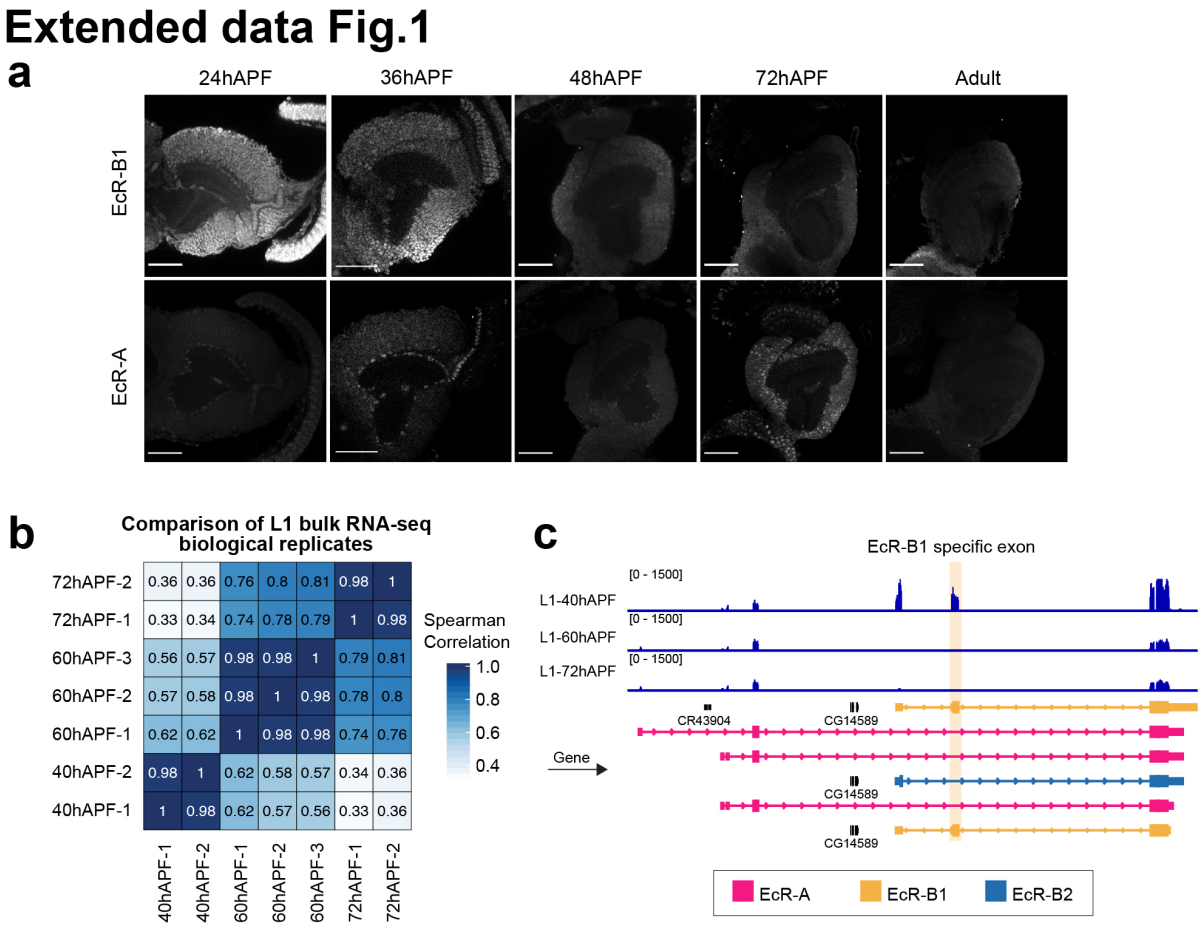

Extended data Fig. 1. | Development change from EcR-B1 to EcR-A isoform. a, Staining using anti-EcR-B1 or anti-EcR-A antibodies at the indicated times in development. Scale bar, 50μm. Note: EcR-A positive cells at 36hAPF are glia. **b,** Comparison of replicates of bulk RNA-Seq of L1 neurons at 40hAPF, 60hAPF and 72hAPF. Values given are Spearman correlation values (see Methods). **c,** Coverage tracks from L1 bulk RNA-Seq in the EcR locus at 40hAPF, 60hAPF and 72hAPF. EcR-A, EcR-B1 and EcR-B2 transcripts are shown, and EcR-B1 specific exon is highlighted.

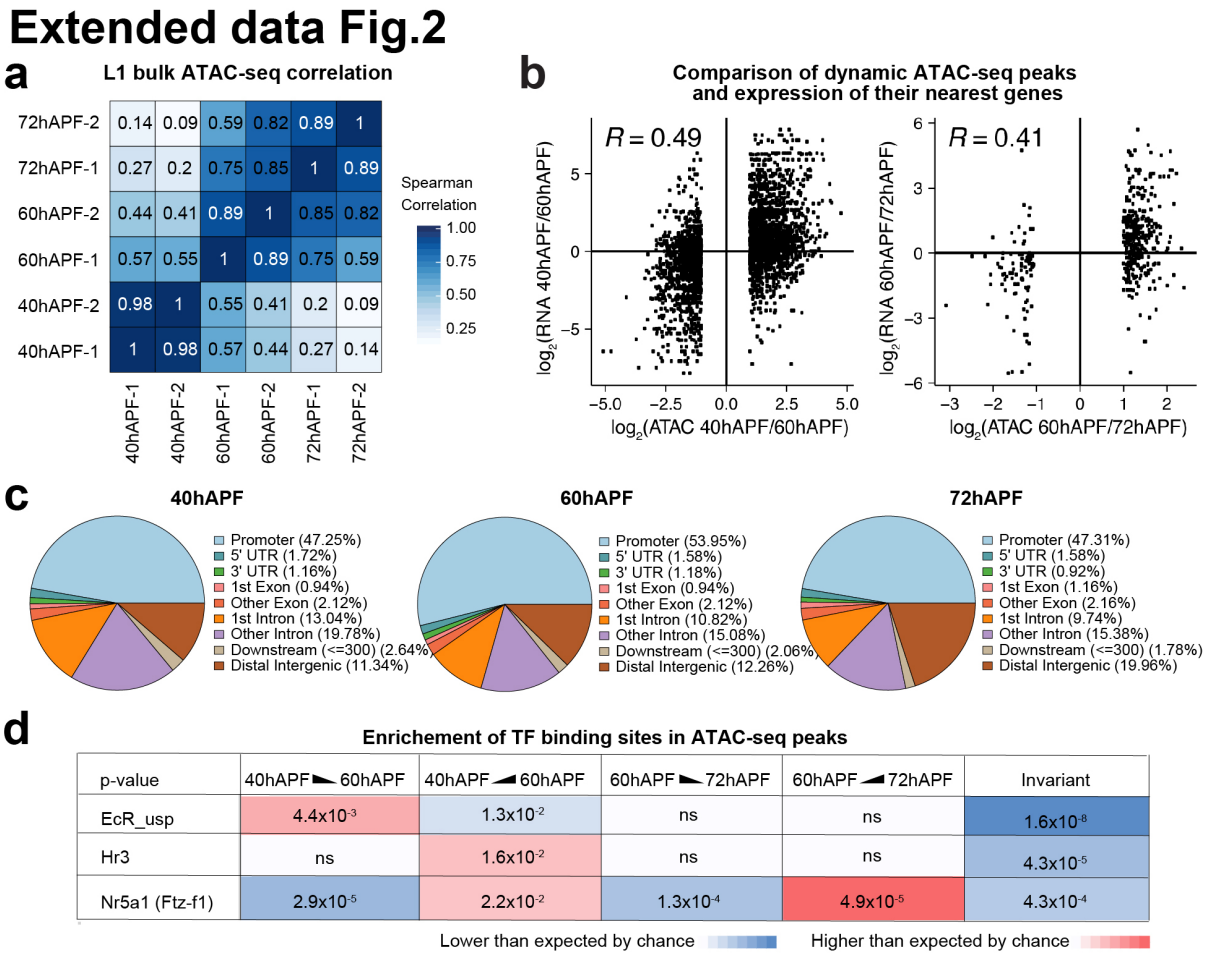

Extended data Fig. 2. | ATAC-Seq analysis of developing L1. a, Comparison of replicates of bulk ATAC-Seq data of L1 neurons at 40hAPF, 60hAPF and 72hAPF. Values shown are Spearman correlation values (see Methods). **b,** Comparison of change of ATAC-seq peak coverage (for regions with dynamic coverage over time) and change in expression of nearest gene. $\log_2$(fold change RPKM of nearest gene) vs $\log_2$(fold change ATAC-seq peak coverage) between 40hAPF and 60hAPF, and 60hAPF and 72hAPF. r, Pearson's correlation coefficient. **c,** Distribution of the top 5000 peaks at each time point between various genomic landmarks. **d,** p-values (Hypergeometric test) for enrichment of binding motifs of EcR-usp complex, Hr3 and Nr5a1 (mammalian homolog for Ftz-f1) amongst the following sets of ATAC-Seq peaks: peaks going down from 40hAPF to 60hAPF, peaks going up from 40hAPF to 60hAPF, peaks going down from

692 60hAPF to 72hAPF, peaks going up from 60hAPF to 72hAPF, and peaks invariant over time. Red:
693 occurrence of motif is higher than expected by chance, blue: occurrence of motif is lower than
694 expected by chance (see Methods).

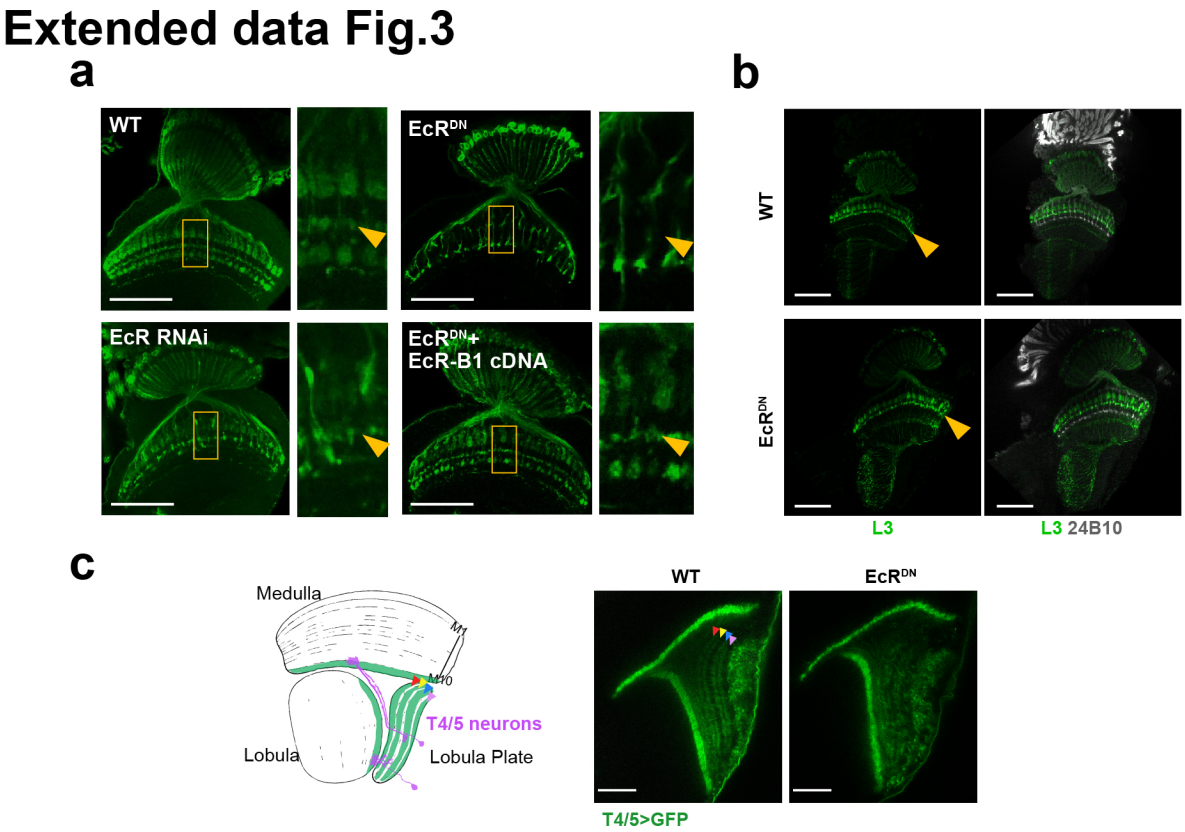

695 **Extended data Fig. 3. | Analysis of morphology with or without EcR^{DN} expression. a,**
696 Morphology of lamina neurons (L1-L5) in wildtype (WT) brains and upon pan-lamina expression
697 (using 9B08 Gal4) of EcR^{DN}, EcR^{DN} + EcR-B1 cDNA or EcR RNAi. Arrowhead in inset points
698 to M3 medulla layer. Note: loss of arborization in M3 with EcR^{DN} is likely due to loss of driver
699 expression in L3 neurons (see Extended data Fig. 3b). **b,** Morphology of L3 neurons with or
700 without EcR^{DN} expression using an L3-specific driver (9D03 Gal4). Note, in adults 9D03 Gal4
701 also labels some L2 neurons. This is not the case during development (see Extended data Fig. 16b,
702 c) **a, b,** Arrowhead points to M3 layer in the medulla. Scale bar, 50μm. **c,** Effect of EcR^{DN}
703 expression on morphology of T4/T5 neurons. Four layers in the lobula plate, a, b, c and d, are
704 marked with red, yellow, blue and pink arrowheads, respectively. Cartoons of one T4 (purple

705 neuron, top) and one T5 neuron (purple neuron, bottom) are shown to highlight wildtype

706 morphology. Scale bar, 20μm.

Extended data Fig.4

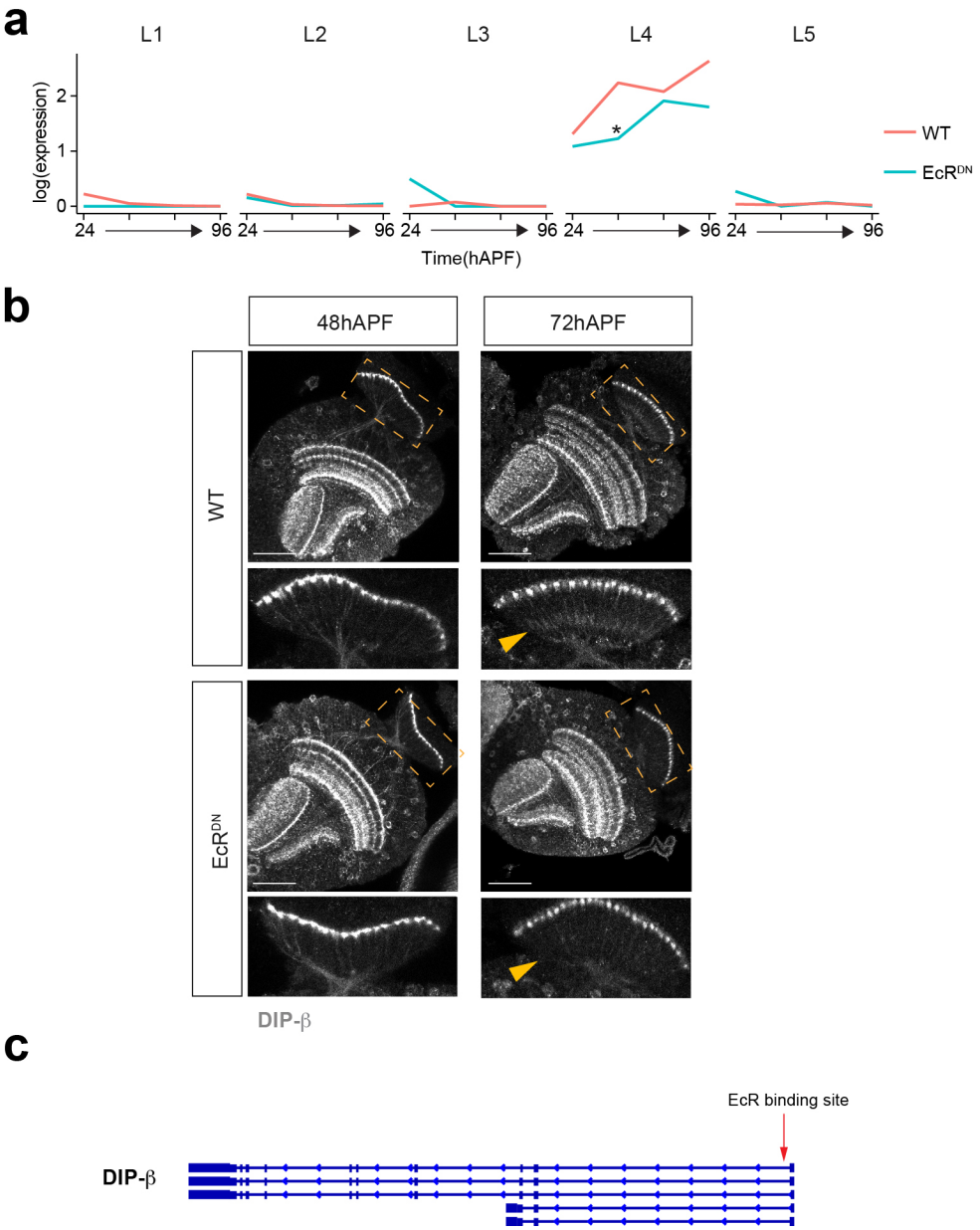

Extended data Fig. 4. | DIP-β expression with or without EcR^{DN}. a, DIP-β mRNA expression in L1-L5 neurons across development with or without pan-lamina expression of EcR^{DN} (from scRNA-Seq based transcriptomic analyses, see Fig. 3, Extended data Fig. 7, 8). * significant difference between control and EcR^{DN} (change in expression > 2fold, p-value < 0.05). **b,** Staining using anti-DIP-β antibody at the indicated time points in development with or without pan lamina

712 expression of EcR^{DN}. Inset shows the lamina neuropil. Arrowhead points to proximal lamina
713 neuropil, positive for DIP-β staining at 72hAPF. Note that staining is largely absent from the
714 lamina neuropil (yellow arrowheads). The level of DIP-β RNA is reduced in EcR^{DN} at 48 but rises
715 to near normal levels again at 72 hrs. We assume that the decrease in RNA leads to a lag in the
716 accumulation of DIP-β protein. **c,** EcR-usp complex binding motif within the first intron of DIP-
717 β (FDR < 10^{-7}, see Methods).

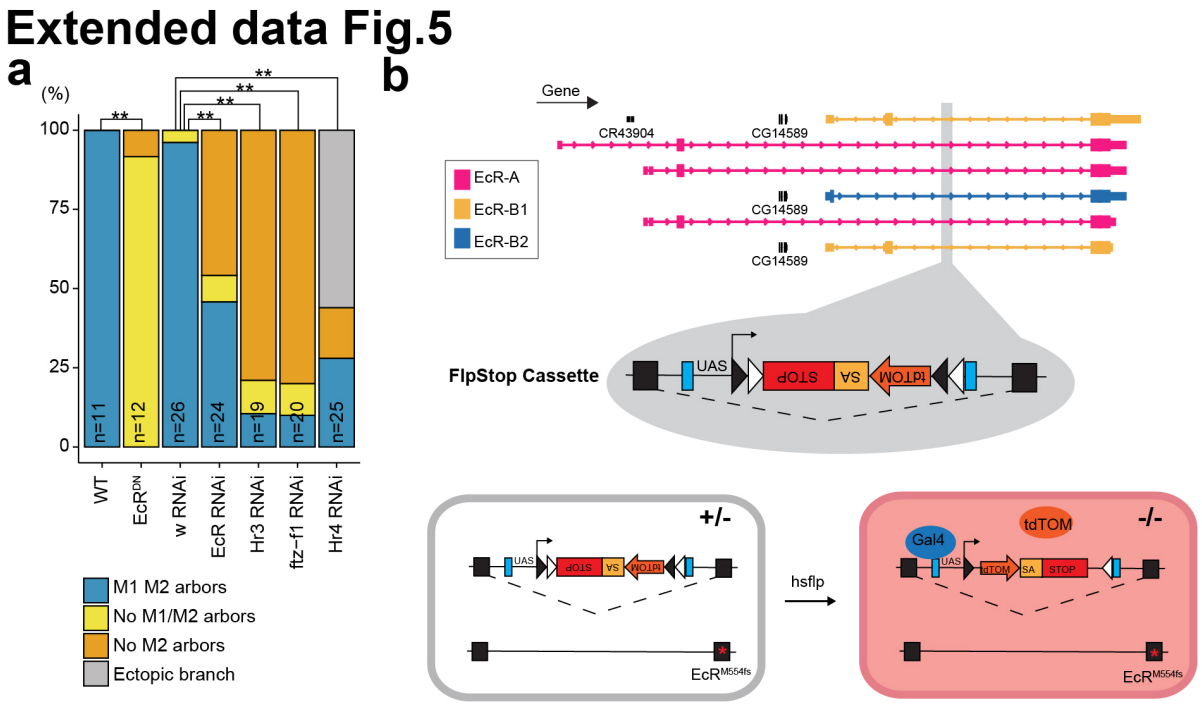

718 **Extended data Fig. 5. | Cell and cell-type autonomous analysis of EcR function. a,** Different
719 L5 arborization defects and their distributions under the given genotypes (see Fig. 2g). All
720 transgenes are expressed using an L5-specific driver (pan-lamina driver is used for data in Fig.
721 2g). n = number of neurons (all conditions, animals ≥ 4). **, p-value < 0.001. **b,** schematic showing
722 the $EcR^{FlpStop}$ allele. FlpStop cassette is inserted in the first common intron of EcR (grey bar shows
723 insertion site, Mi{MIC}EcRMI05320). Cells expressing Gal4, within which a stochastic, heat-
724 shock FLP recombinase-mediated flipping of the cassette occurs, express tdTom.

Extended data Fig.6

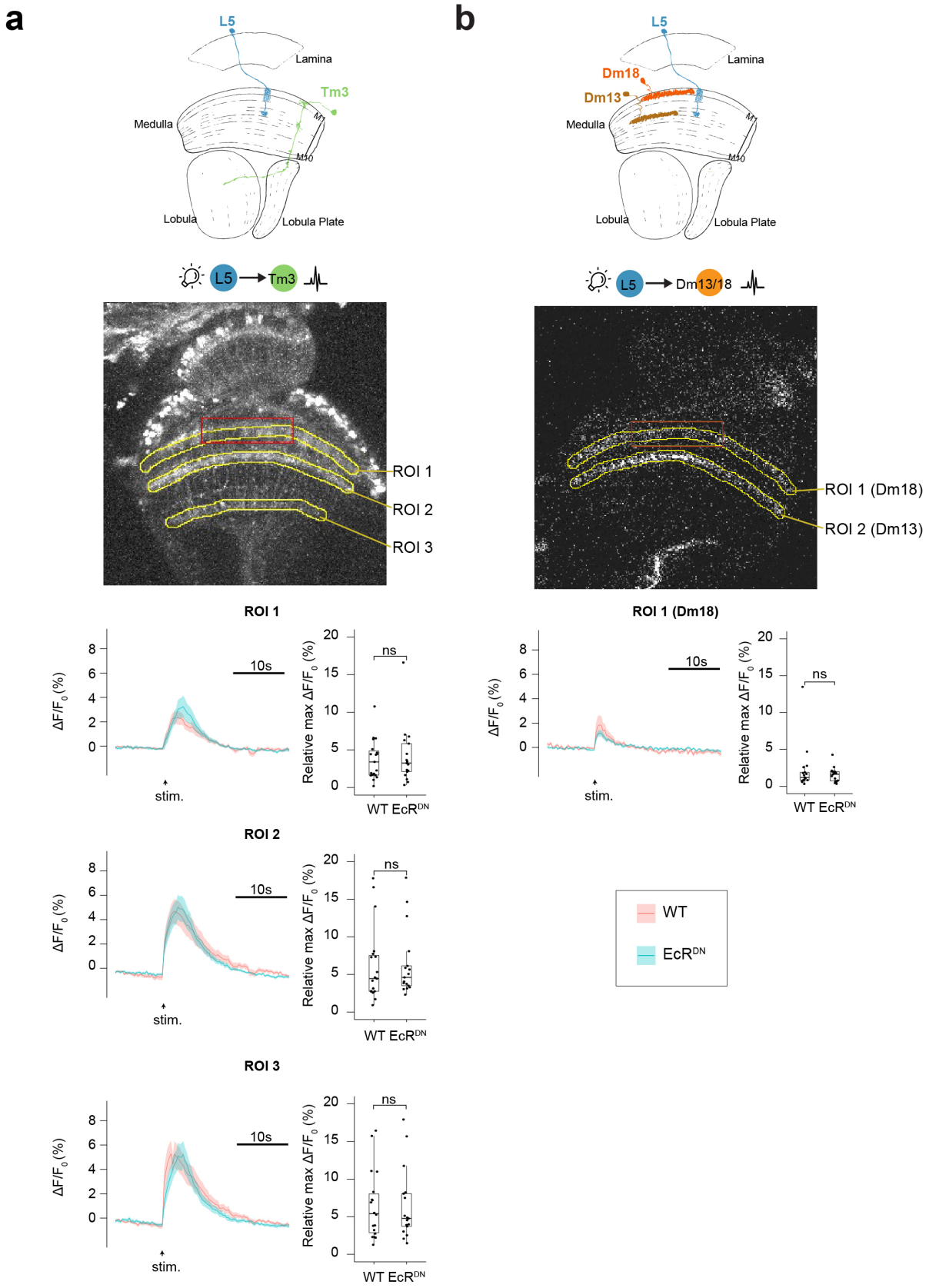

725 **Extended data Fig. 6. | Optogenetics-based assay for communication between L5 and its**
726 **postsynaptic partners. a,** Ca^{2+} response from Tm3 (measured using GCaMP6s) upon optogenetic
727 stimulation of L5 with (blue line) or without (red line) EcR^{DN} expression in L5. GCaMP6s
728 responses were measured in 3 regions of interest (ROI). ROI 1, ROI 2 and ROI 3 span medulla
729 layers M1, M5 and M10 respectively. (WT, 19 animals; EcR^{DN}, 17 animals.) **b,** Ca^{2+} response
730 from Dm13 and Dm18 (common LexA driver used yields expression in both Dm13 and Dm18,
731 see Extended data Table 1) upon optogenetic stimulation of L5 with (blue line) or without (red
732 line) EcR^{DN} expression in L5. ROI 1 spans M1 and measures response from Dm18. ROI 2 spans
733 M5 and measures response from Dm13. (WT, 19 animals; EcR^{DN}, 17 animals.) Note: weak
734 response from Dm18 upon stimulation of L5 irrespective of condition. **a, b,** Amplitude of relative
735 peak response for each condition is quantified. There is no significant difference between WT and
736 EcR^{DN} for any comparison shown here. For Dm13 response, see Fig. 2j.

Extended data Fig.7

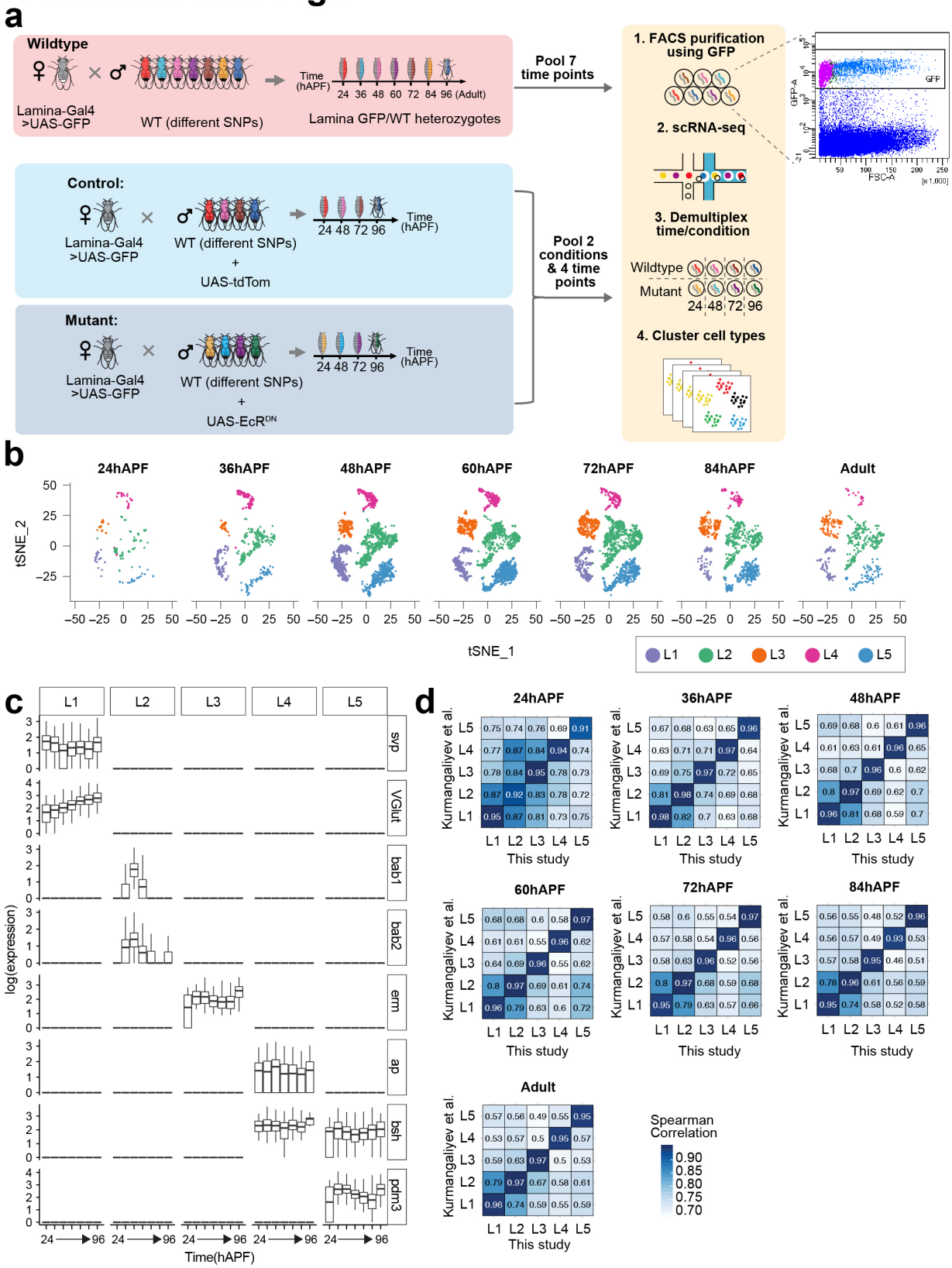

737 **Extended data Fig. 7. | Approach for identification of EcR and Hr3 targets using scRNA-**
738 **Seq. a,** Scheme for scRNA-Seq based transcriptomic analysis of WT and mutant lamina neurons
739 (see Kurmangaliyev *et al.*[12] and methods). GFP vs forward scatter 2-D plot showing criteria used
740 to enrich for lamina neurons by FACS is shown on the right. 'Cells' highlighted in purple were
741 excluded despite being GFP+ due to their small size. **b,** tSNE plots showing WT L1-L5 clusters at
742 24, 36, 48, 60, 72, 84 and 96 hAPF (Adult). **c,** Log(expression) of previously identified lamina
743 neuron type-specific genes in L1-L5 clusters identified at each time point over development (see
744 Tan *et al.*[32]). **d,** Comparison of lamina neuron transcriptomes generated by scRNA-Seq in this
745 study and by scRNA-Seq in Kurmangaliyev *et al.* Values given are Spearman correlation values.

Extended data Fig.8

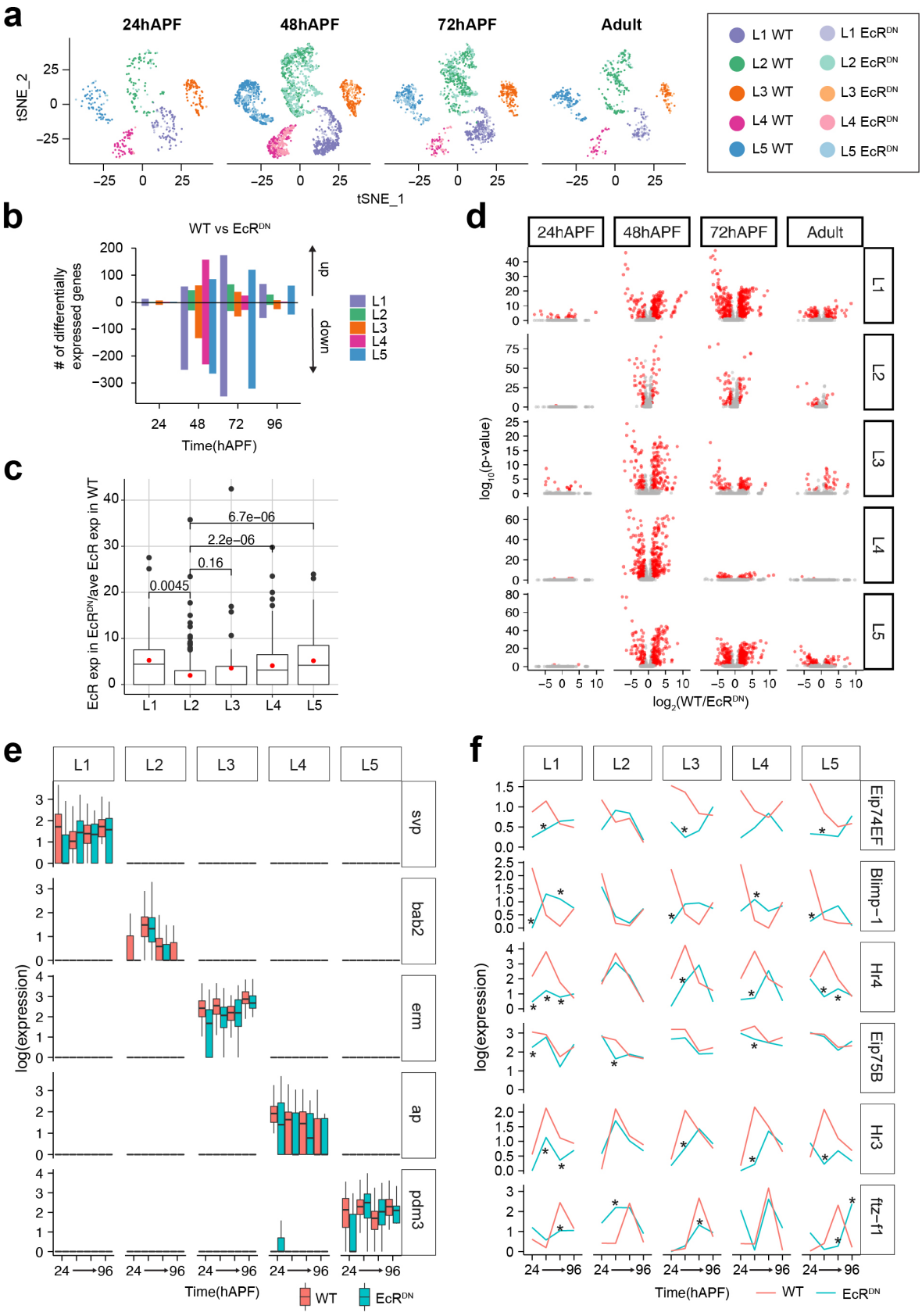

746 **Extended data Fig. 8. | scRNA-Seq-based analysis of WT and EcR^{DN} expressing lamina**
747 **neurons. a,** tSNE plots showing WT and EcR^{DN}-expressing L1-L5 clusters at 24, 48, 72 and 96
748 hAPF (Adult). **b**, Number of genes up or downregulated in EcR^{DN} in L1-L5 neurons. **c,** Expression
749 of EcR in EcR^{DN}-expressing lamina neurons at 48hAPF normalized to mean expression of EcR in
750 wildtype cells at 48hAPF (done separately for each lamina neuron-type). Red dots, mean of data
751 spread. Increase in EcR expression in EcR^{DN}-expressing cells over wildtype is expected to be due
752 to the expression of the EcR^{DN} transgene. Note the poor induction of EcR^{DN} in L2 neurons. p-value
753 from student's t-test are stated in the figure for comparison between L2 and other lamina neuron-
754 types. The difference between EcR^{DN} expression in L2 and L3 neurons is not significant likely due
755 to the low cell numbers of EcR^{DN}-expressing L3 neurons. **d,** Volcano plots showing significant
756 gene expression changes in L1-L5 neurons throughout development. Red dots: fold change > 2
757 and p-value < 0.05. **e,** Log(expression) of lamina neuron-type specific TFs with (blue) or without
758 (red) EcR^{DN}. Note no change in expression of TFs ± EcR^{DN}. **f,** Log(expression) of TFs in the
759 Ecdysone-pathway in WT (red lines) and EcR^{DN}-expressing (blue lines) L1-L5 neurons. *, p-value
760 < 0.05, fold change > 2.

Extended data Fig.9

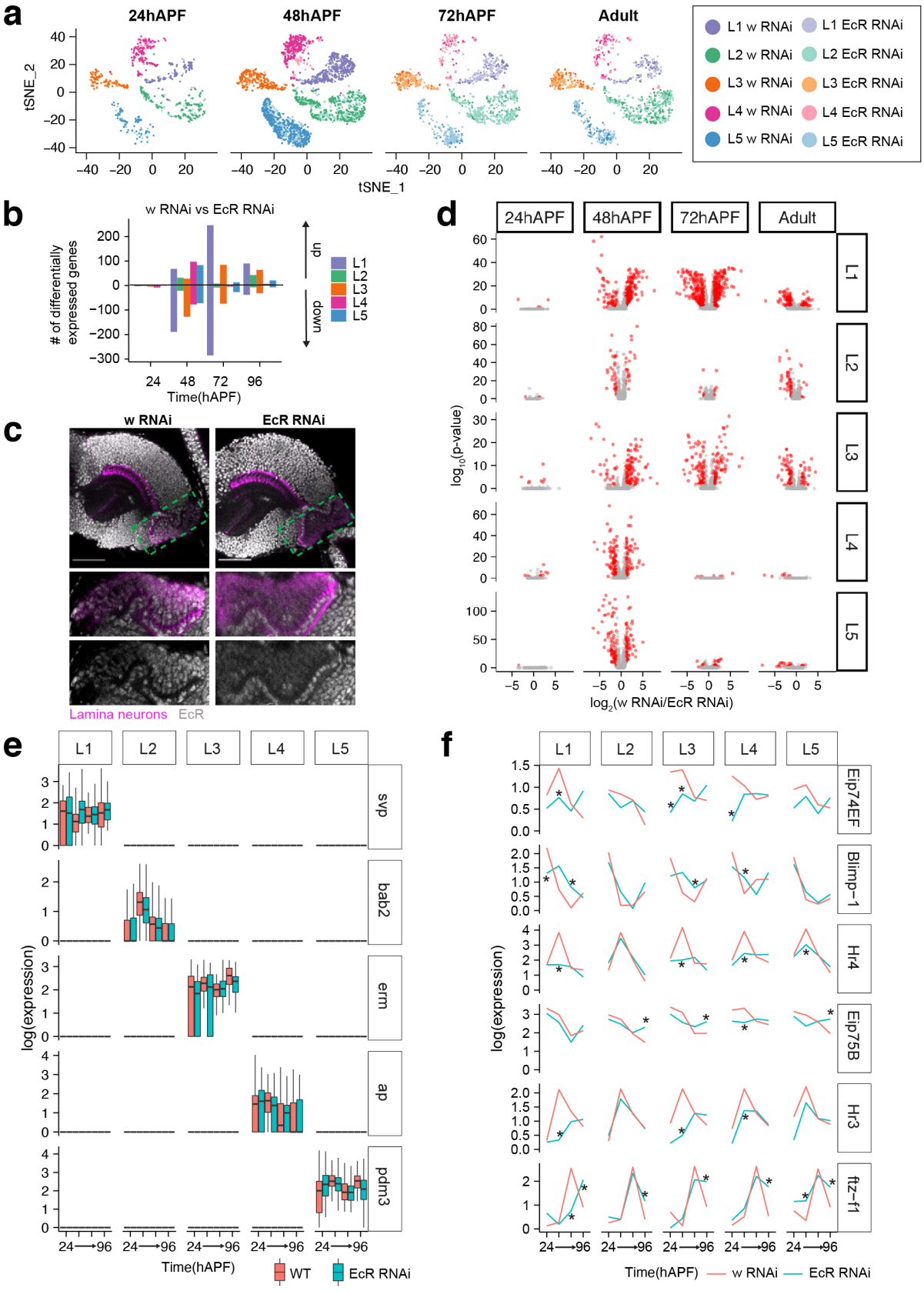

761 **Extended data Fig. 9. | scRNA-Seq-based analysis of w RNAi and EcR RNAi expressing**
762 **lamina neurons. a,** tSNE plots showing w RNAi and EcR RNAi-expressing L1-L5 clusters at 24,
763 48, 72 and 96 hAPF (Adult). **b**, Number of genes up or downregulated in EcR RNAi in L1-L5
764 neurons. **c,** Image showing optic lobe (top) stained using an antibody targeting all EcR isoforms
765 (grey) at 24hAPF. Box with green dotted outline marks the region containing lamina neuron cell-
766 bodies. This region is magnified in bottom two panels. Lamina neurons are labeled in magenta.
767 Scale bar, 50μm. **d,** Volcano plots showing significant gene expression changes in L1-L5 neurons
768 throughout development. Red dots: fold change > 2 and p-value < 0.05. **e,** Log(expression) of
769 lamina neuron-type specific TFs with (blue) or without (red) EcR RNAi. Note no change in
770 expression of TFs ± EcR RNAi. **f,** Log(expression) of TFs in the Ecdysone-pathway in WT (red
771 lines) and EcR RNAi-expressing (blue lines) L1-L5 neurons. *, p-value < 0.05, fold change > 2.

Extended data Fig.10

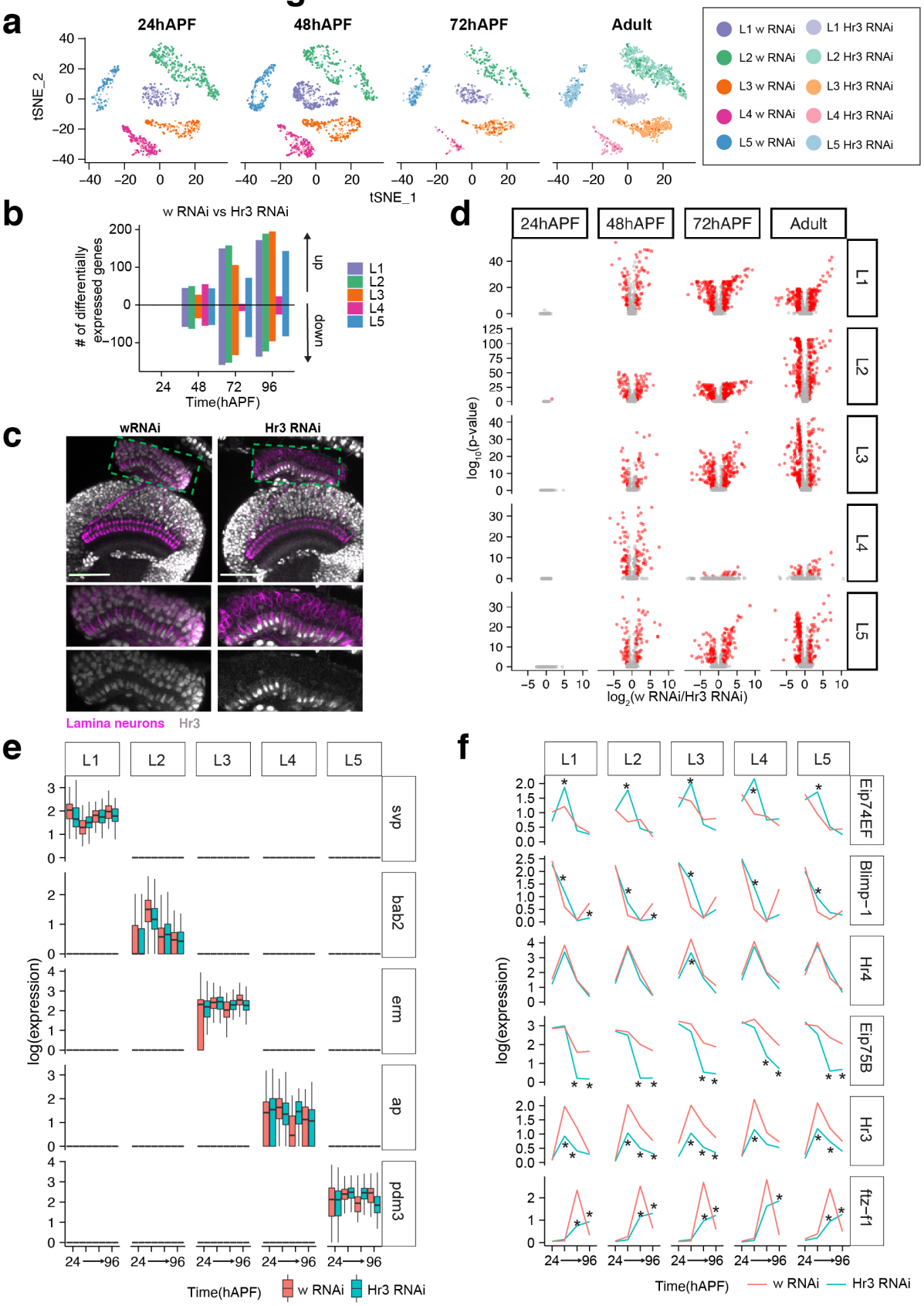

772 **Extended data Fig. 10. | scRNA-Seq-based analysis of w RNAi and Hr3 RNAi expressing**
773 **lamina neurons. a,** tSNE plots showing w RNAi and Hr3 RNAi-expressing L1-L5 clusters at 24,
774 48, 72 and 96 hAPF (Adult). **b**, Number of genes up or downregulated in Hr3 RNAi in L1-L5
775 neurons. **c,** Image showing optic lobe (top) stained using an antibody targeting Hr3 (grey) at
776 24hAPF. Box with green dotted outline marks the region containing lamina neuron cell-bodies.
777 This region is magnified in bottom two panels. Lamina neurons are labeled in magenta. Scale bar,
778 50µm. **d,** Volcano plots showing significant gene expression changes in L1-L5 neurons throughout
779 development. Red dots: fold change > 2 and p-value < 0.05. **e,** Log(expression) of lamina neuron-
780 type specific TFs with (blue) or without (red) Hr3 RNAi. Note no change in expression of TFs ±
781 Hr3 RNAi. **f,** Log(expression) of TFs in the Ecdysone-pathway in WT (red lines) and Hr3 RNAi-
782 expressing (blue lines) L1-L5 neurons. *, p-value < 0.05, fold change > 2.

Extended data Fig.11

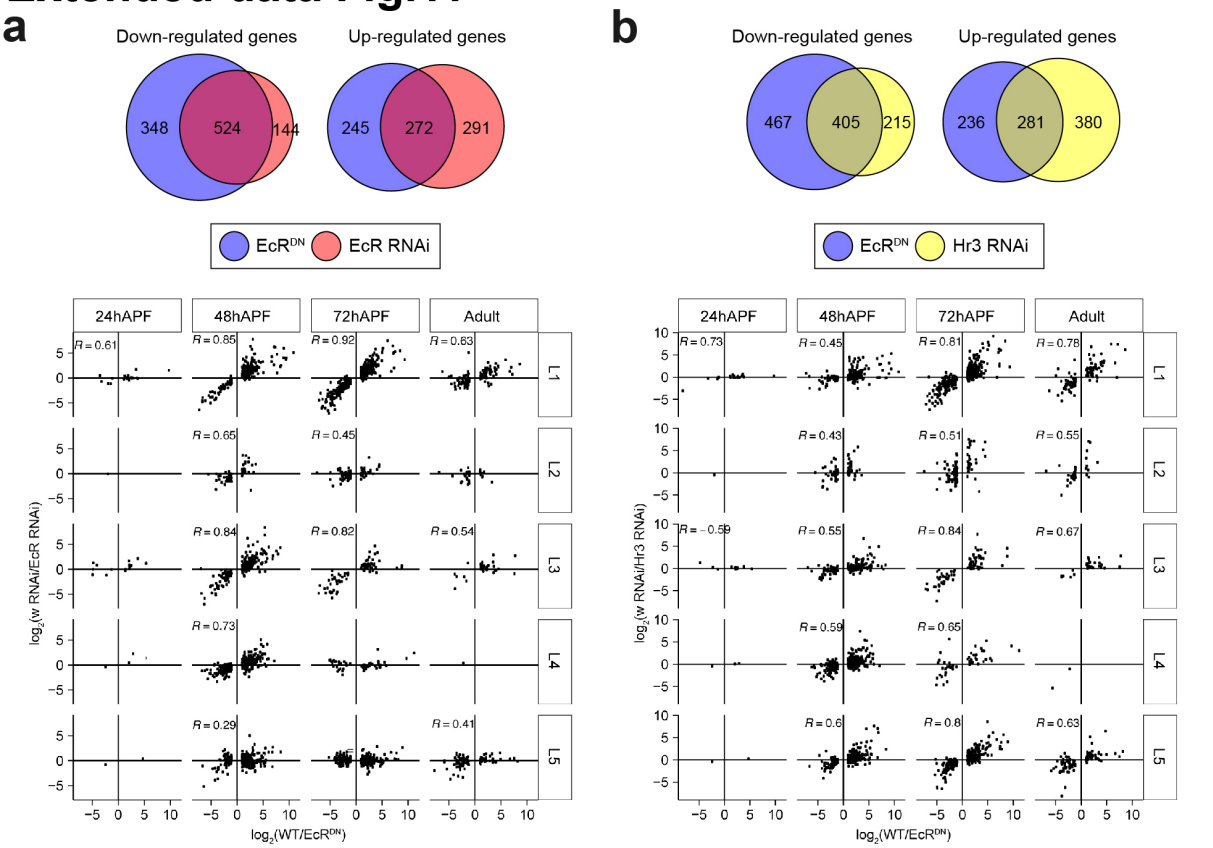

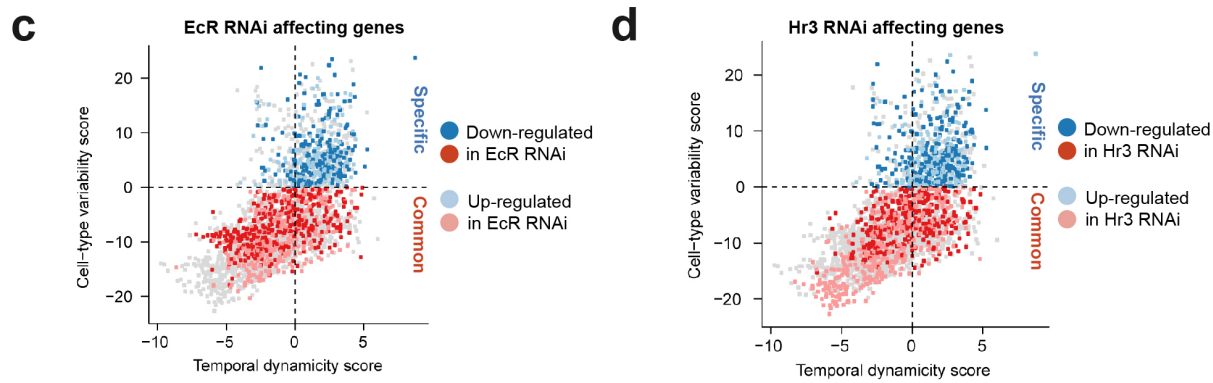

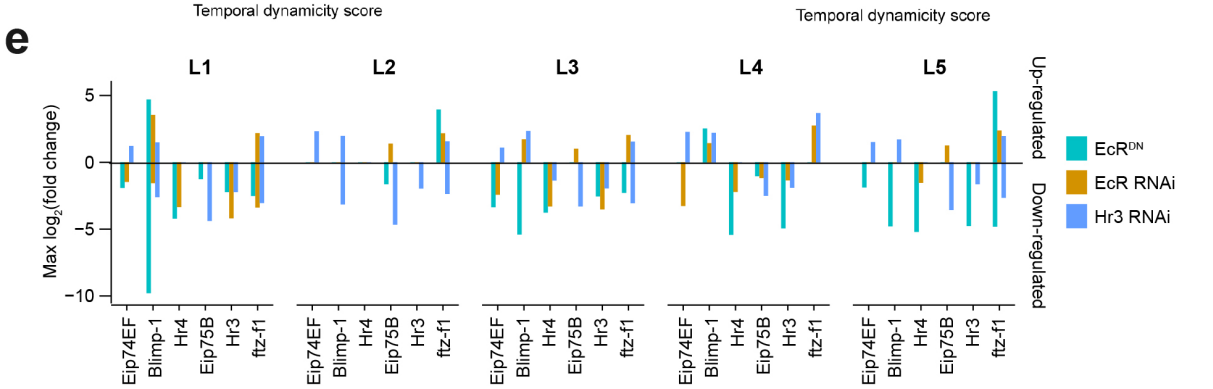

783 **Extended data Fig. 11. | Comparison of genes affected by EcR^{DN}, EcR RNAi and Hr3 RNAi.**
784 **a,** Top, Venn diagram showing overlap between genes downregulated by EcR^{DN} and EcR RNAi
785 across all time points and lamina neuron-types. Below, log_2(normalized expression in w
786 RNAi/EcR RNAi) vs log_2(normalized expression in WT/EcR^{DN}) for L1-L5 neurons throughout
787 development. Correlation coefficient, R, is given for comparisons where $p < 0.05$. **b,** Top, Venn
788 diagram showing overlap between genes downregulated by EcR^{DN} and Hr3 RNAi across all time
789 points and lamina neuron-types. Below, log_2(normalized expression in w RNAi/Hr3 RNAi) vs
790 log_2(normalized expression in WT/EcR^{DN}) for L1-L5 neurons throughout development.
791 Correlation coefficient, R, is given for comparisons where $p < 0.05$. **c,** Cell-type variability vs
792 Temporal dynamicity plot for EcR RNAi-affected genes (fold change > 2, p-value < 0.05). Cell-
793 type Specific (blue) and Common (red) targets are shown. Darker colors: genes reduced in EcR
794 RNAi, lighter colors: genes increased in EcR RNAi. **d,** Cell-type variability vs Temporal
795 dynamicity plot for Hr3 RNAi-affected genes (fold change > 2, p-value < 0.05). Cell-type Specific
796 (blue) and Common (red) targets are shown. Darker colors: genes reduced in Hr3 RNAi, lighter
797 colors: genes increased in Hr3 RNAi. **e,** Maximum change in expression of Ecdysone-pathway
798 TFs in L1-L5 neurons with EcR^{DN}, EcR RNAi and Hr3 RNAi. Note that EcR RNAi often has
799 weaker effect on TF expression as compared to EcR^{DN}.

Extended data Fig.12

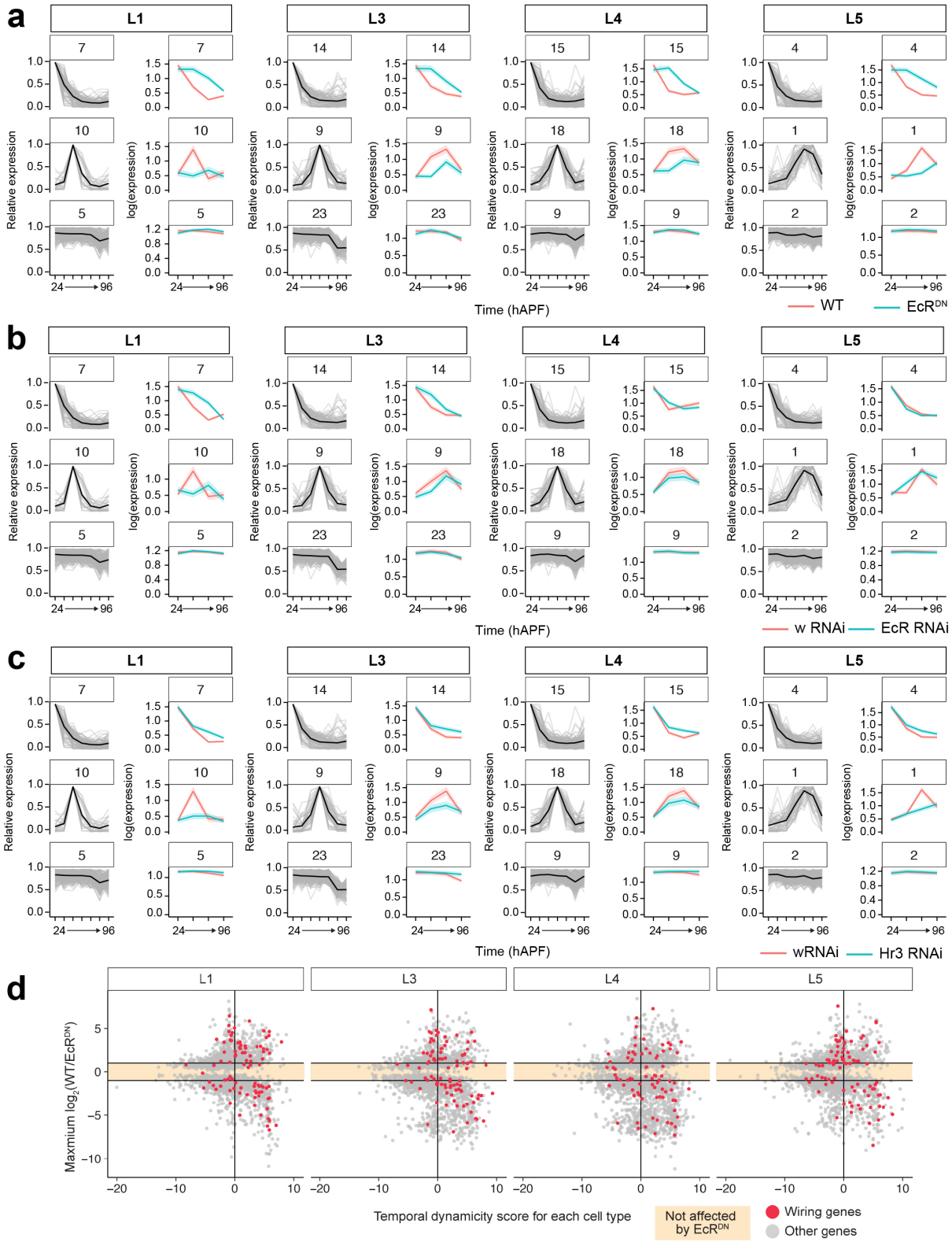

800 **Extended data Fig. 12. | Clusters of genes most affected by EcR^{DN}, EcR RNAi and Hr3 RNAi.**
801 All genes expressed in L1-L5 neurons (done separately for each cell-type) were clustered into
802 groups (using k-means clustering) based on their expression dynamics (see Methods). Clusters that
803 show maximum upregulation or downregulation with EcR^{DN} are shown in **a – c (**clusters are
804 indicated in numbers above each graph). Also shown are clusters unchanged by EcR^{DN}. For each
805 panel: left, light grey lines, relative expression of all genes in the cluster; black line, mean of
806 relative expression of all genes in the cluster. Right, red line, mean relative expression in control;
807 blue line, mean relative expression with perturbation. Shades are SEM. d, examples of dynamic
808 wiring genes that are not affected by EcR^{DN}. **d,** Plots showing maximum change in expression
809 [$\log_2(WT/EcR^{DN})$] caused by EcR^{DN} vs the temporal dynamicity of the gene (calculated separately
810 for each cell-type). Shown in red are wiring genes. Colored region on the plot represents genes not
811 affected by EcR^{DN}. Note many genes including wiring genes (especially in L1, L3 and L4) with
812 high temporal dynamicity scores that are not affected by EcR^{DN}.

Extended data Fig.13

a

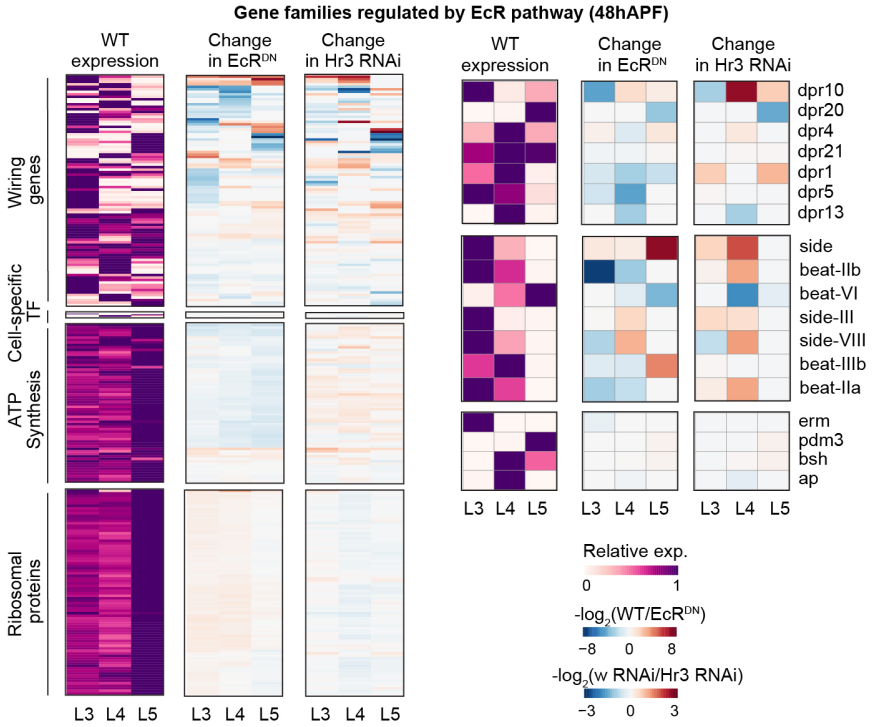

b

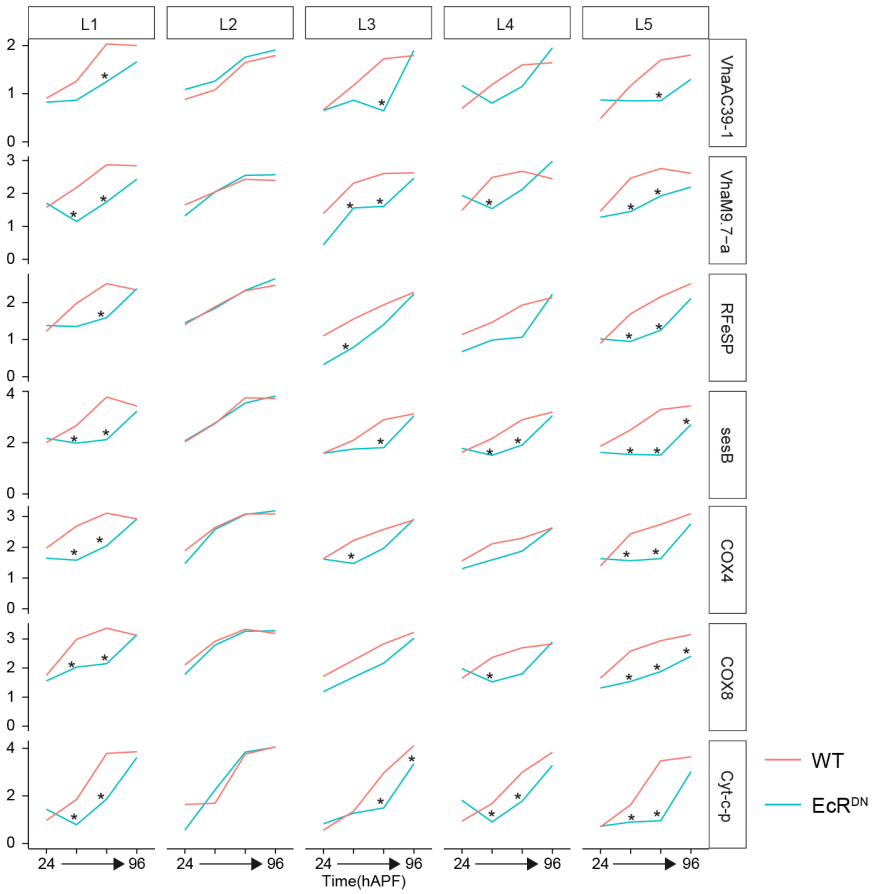

813 **Extended data Fig. 13. | Families of genes affected by EcR^{DN} and Hr3 RNAi. a,** Relative WT
814 expression (left), change in expression with EcR^{DN} (center), and change in expression with Hr3
815 RNAi (right) shown as heat maps for all genes expressed in L3-L5 neurons belonging to the
816 specified gene categories at 48hAPF (also see Extended data Fig. 13). Examples of genes
817 belonging to the Dpr family, Side-Beat family and cell-type specific transcription factors are
818 shown separately. **b,** Expression of some genes involved in ATP synthesis and vacuolar ATPase
819 biology are shown with and without EcR^{DN} in L1-L5 neurons across development. *, fold change
820 between WT and $EcR^{DN} > 2$, p-value < 0.05. Note: expression in adults is not significantly affected
821 by EcR^{DN}.

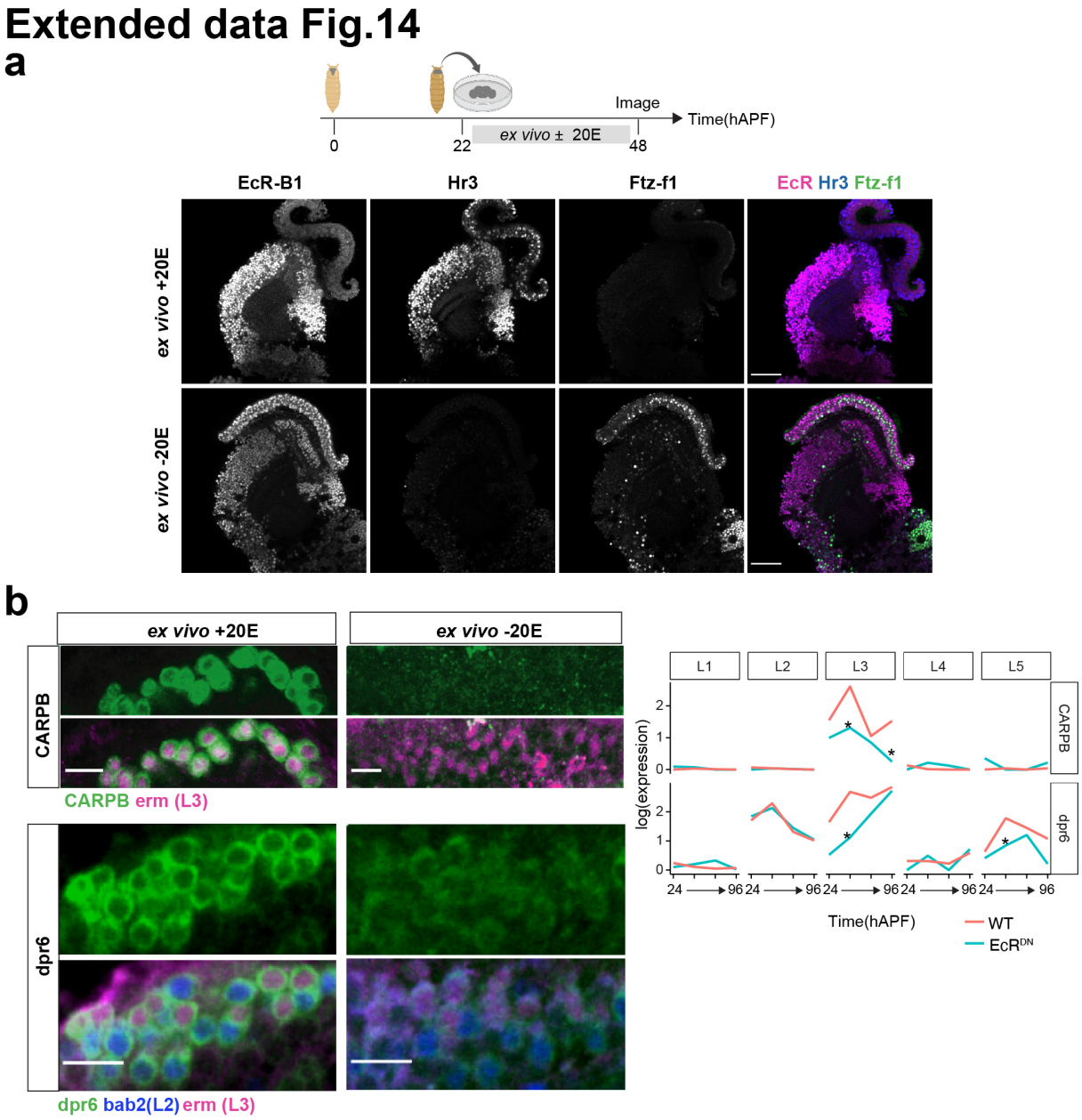

822 **Extended data Fig. 14. | *ex vivo* culture of pupal brain with or without Ecdysone. a,** Top,
823 schematic of experimental setup (see Methods). Briefly, brains are dissected at 22hAPF then
824 incubated for 26h in media ± 20E (20 HydroxyEcdysone, active form of Ecdysone). Bottom, optic
825 lobes stained for EcR-B1, Hr3 and Ftz-f1 cultured *ex vivo* ± 20E. Scale bar, 50µm. **b,** Left, Staining
826 for CARPB and dpr6 reporters (MiMIC lines, see Methods) in lamina neuron cell-bodies ± 20E.

827 Right, CARPB and dpr6 expression with (blue) or without (red) EcR^{DN}. *, fold change between
828 WT and EcR^{DN} > 2, p-value < 0.05. Note: dpr6 expression is unchanged in L2 with pan-lamina
829 expression of EcR^{DN}, however staining in brains cultured *ex vivo* without 20E in the medium shows
830 reduced protein expression in L2 (bab2 positive cell-bodies). This is consistent with weak activity
831 of the pan-lamina driver (9B08 Gal4) in L2 at 48hAPF leading to ineffective inhibition of the
832 Ecdysone-pathway (see Extended data Fig. 8c).

Extended data Fig.15

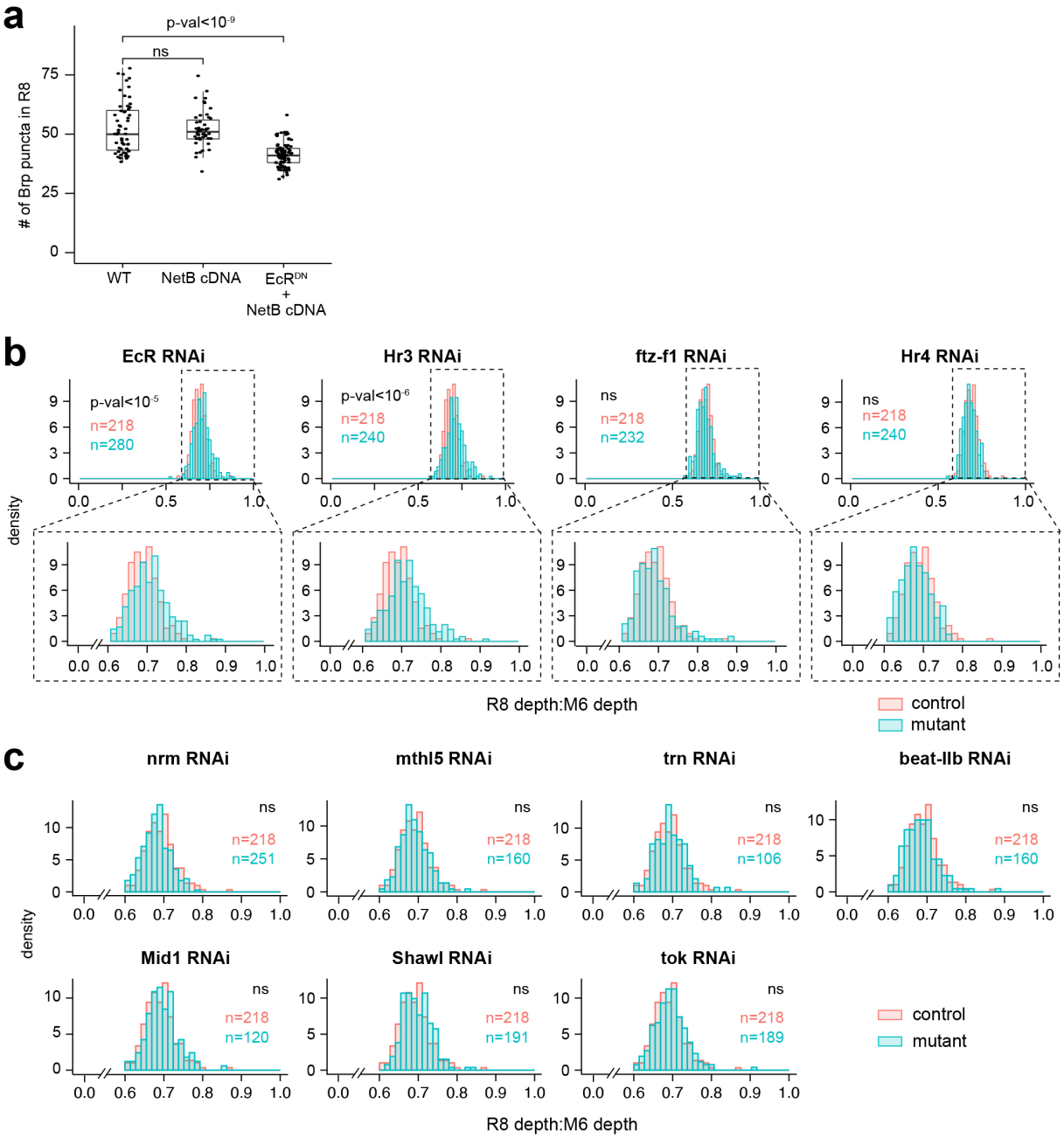

Extended data Fig. 15. | Genes expressed in L3 required for R8 wiring. a, Total number of presynaptic sites (Brp puncta) in R8 neurons with WT, NetB overexpressing, or EcR^{DN} and NetB-expressing L3 neurons. NetB overexpression is unable to rescue the reduction in R8 presynaptic sites seen with expression of EcR^{DN} in L3 neurons (see Fig. 4c). p-value (Student's t-test) is given. **b, c,** Distributions of R8 axon terminal depth in w RNAi (red) or with expression of other RNAi

838 (as shown, blue) in L3 neurons. All conditions, number of animals ≥ 3. p-values (Kolmogorov-
839 Smirnov test) are given. ns = Not significant. **b,** RNAi against TFs in the Ecdysone-pathway. **c,**
840 Results from RNAi screen showing genes that did not significantly affect R8 axon depth. Numbers
841 of neurons/ condition are given.

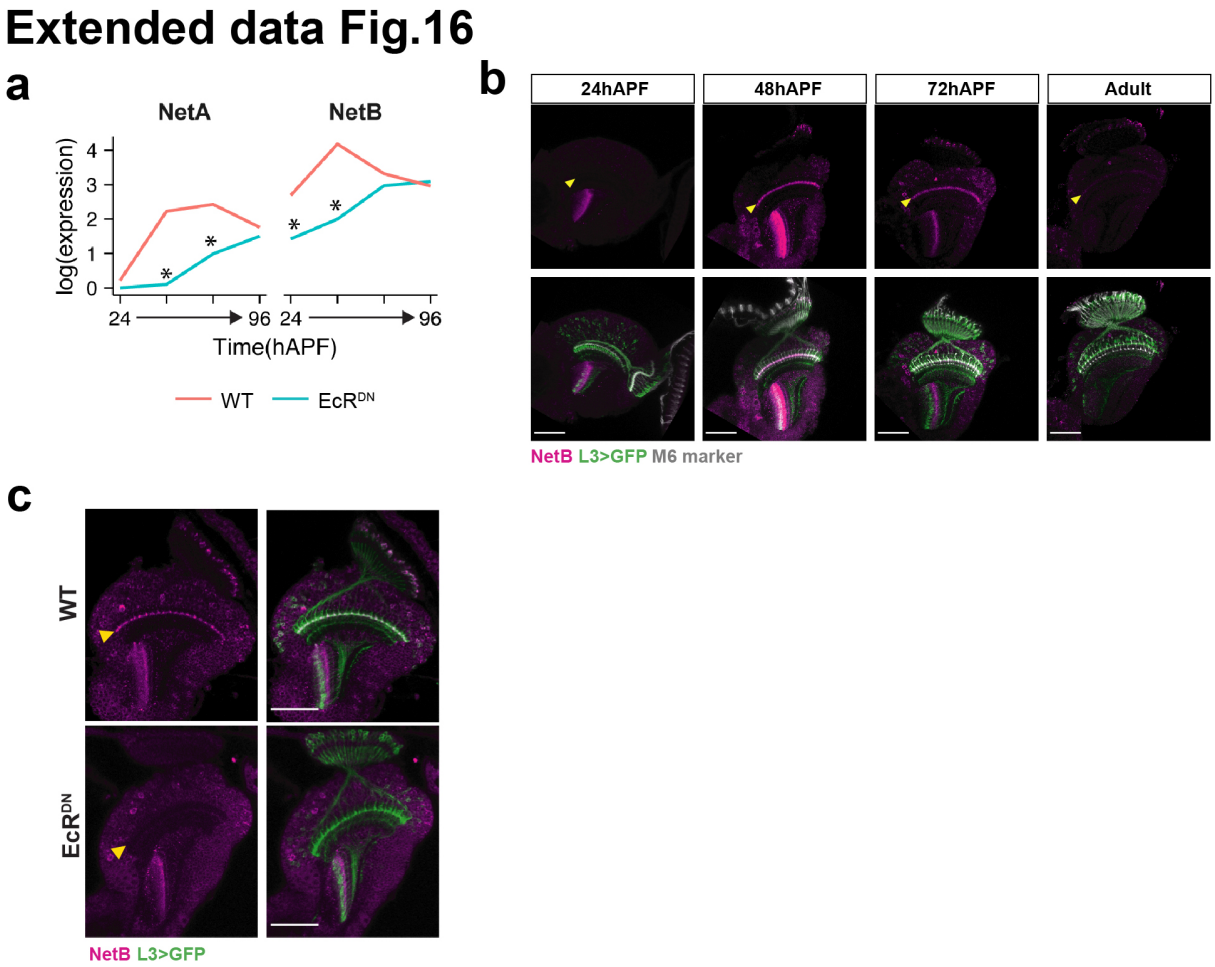

Extended data Fig. 16. | Netrin expression in L3 requires EcR activity. a, Expression of NetA and NetB in L3 with (blue) or without (red) EcR^{DN} expression. *, fold change between WT and EcR^{DN} > 2, p-value < 0.05. **b,** Staining using anti-NetB antibody (magenta) at the indicated times in development. Marker for M6 medulla layer (24B10, grey) and L3 neurons labeled with GFP (green) are shown. **c,** Staining using anti-NetB antibody (magenta) ± EcR^{DN} expression only in L3. L3 neurons labeled with GFP (green) are shown. **b, c,** Scale bar, 50μm. Yellow arrowhead, M3 medulla layer.

849 **Additional References**

850 58. Picelli, S. *et al.* Full-length RNA-seq from single cells using Smart-seq2. *Nat Protoc* **9**, 171–
851 181 (2014).
852 59. Buenrostro, J. D., Giresi, P. G., Zaba, L. C., Chang, H. Y. & Greenleaf, W. J. Transposition
853 of native chromatin for fast and sensitive epigenomic profiling of open chromatin, DNA-binding
854 proteins and nucleosome position. *Nat Methods* **10**, 1213--1218 (2013).
855 60. Ambrosini, G., Groux, R. & Bucher, P. PWMScan: a fast tool for scanning entire genomes
856 with a position-specific weight matrix. *Bioinformatics* **34**, 2483–2484 (2018).
857 61. Butler, A., Hoffman, P., Smibert, P., Papalexi, E. & Satija, R. Integrating single-cell
858 transcriptomic data across different conditions, technologies, and species. *Nat Biotechnol* **36**,
859 411–420 (2018).
860 62. Xu, S. *et al.* Interactions between the Ig-Superfamily Proteins DIP-α and Dpr6/10 Regulate
861 Assembly of Neural Circuits. *Neuron* **100**, 1369--1384.e6 (2018).

862 **Extended data Tables**

863 **Extended data Table 1.** Fly strains used in this study

864 **Extended data Table 2.** Temporal dynamicity and cell-type variability scores

865 **Extended data Table 3.** Wiring genes

866 **Extended data Table 4.** Gene ontology and Reactome analyses

867 **Extended data Table 5.** L1 bulk ATAC-Seq

868 **Extended data Table 6.** scRNA-Seq data for wildtype Lamina neurons

869 **Extended data Table 7.** scRNA-Seq data for wildtype vs EcR^{DN}-expressing Lamina neurons

870 **Extended data Table 8.** scRNA-Seq data for wildtype vs EcR RNAi-expressing Lamina neurons

871 **Extended data Table 9.** scRNA-Seq data for wildtype vs Hr3 RNAi-expressing Lamina neurons

872 **Acknowledgements**

873 We thank Dr. Pecot (Harvard), Dr. Yamanaka (UC Riverside), Dr. Black (UCLA), Dr. De
874 Robertis (UCLA), Dr. Riddiford (Univ. of Washington) and Dr. Truman (Janelia Research
875 Campus) for helpful discussions. We thank Dr. Schuldiner (Weizmann Institute of Science) and
876 members of the Zipursky lab for feedback on the manuscript, and Dr. Diaz de la Loza for help
877 with figure illustrations. We would like to specifically acknowledge Juyoun Yoo's (Zipursky Lab)
878 and Rachel Hodge's (Jones Lab, UCLA) help with ATAC-Seq library prep and immunostaining.
879 We also thank the BSCRC Sequencing Core (UCLA) and the TCGB core (UCLA) for help with
880 library preparation and sequencing; the BSCRC FACS core (UCLA) and the Witte lab (UCLA)
881 for assistance with FACS purification of lamina neurons; and the IDRE Statistics Consulting
882 (UCLA) and Dr. Balliu (UCLA) for assistance with the statistical analysis of data. Reagents
883 provided by Dr. Akin (UCLA), Dr. Laski (UCLA), Dr. Wang (Duke-NUS), Dr. Pecot (Harvard),
884 Dr. Thummel (Univ. of Utah) and Dr. Bashaw (Univ. of Penn.), and fly lines from the Bloomington
885 Drosophila Stock Center were critical for this work. This work was supported by NIH T32-
886 NS048004 Neurobehavioral Genetics Training Grant (S.J.), Helen Hay Whitney Foundation (S.J.)
887 and Whitcome Fellowship (Y.L.). S.L.Z is an investigator of the Howard Hughes Medical Institute.

888 **Author contributions**

889 S.J., Y.L., Y.Z.K., J.V-A and S.L.Z. designed experiments. S.J., Y.L., P.M., S.A.L, J.V-A and B.P.
890 acquired data. S.J., Y.L., J.V-A and Y.K. analyzed the data. S.J., Y.L. and S.L.Z. wrote the
891 manuscript with input from all co-authors.

892 **Competing interest declaration**

893 The authors declare no competing interests.

894 **Additional information**

895 Supplementary Information is available for this paper. Correspondence and requests for materials

896 should be addressed to: Dr. S. Lawrence Zipursky - lzipursky@mednet.ucla.edu.